Nano Energy 135 (2025) 110674

Contents lists available at ScienceDirect

Nano Energy

journal homepage: www.elsevier.com/locate/nanoen

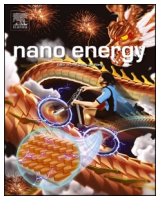

Acoustic energy boosts air purification: A novel sound-wave drive TENG for filterless particulate capturing

Yiting Zhang [a], Siu-Kai Lai [a,b,*], Chen Wang [c], Kin-Fai Ho [d], Chun H. Wang [e]

[a] Department of Civil and Environmental Engineering, The Hong Kong Polytechnic University, Hong Kong, PR China
[b] The Hong Kong Polytechnic University Shenzhen Research Institute, Nanshan, Shenzhen, PR China
[c] Hebei Key Laboratory of Mechanical Reliability for Heavy Equipments and Large Structures, Yanshan University, Hebei, PR China
[d] The Jockey Club School of Public Health and Primary Care, The Chinese University of Hong Kong, Hong Kong, PR China
[e] School of Mechanical and Manufacturing Engineering, The University of New South Wales, Sydney, NSW 2052, Australia

ARTICLE INFO

Keywords:
U-shaped configuration design
Triboelectric nanogenerator
Electrospun nanofiber
Acoustic-driven particle manipulation
Air purification

ABSTRACT

Maintaining good indoor air quality is crucial for human health, as poor air quality in enclosed spaces can elevate the risk of infection and cause premature deaths. This study introduces a novel low-cost, filter-less method for capturing ultrafine particulates to improve air purification efficiency in air ductworks. The new technology employs sound waves to cluster particulates and simultaneously activate triboelectric nanogenerators (TENGs) to operate as electrostatic precipitators, creating a synergistic approach where two techniques complement and enhance each other. The sound waves, created within a U-shaped acoustic resonating chamber using loudspeakers, cluster the particulates and excite the TENG to generate high electrical fields between its electrodes. This high electrical field captures the clustered particulates by electrostatic precipitation. Experimental tests are utilized in this work. The peak electrical output of the electrospun nanofiber-based TENG was recorded at approximately 60 V (peak-to-peak value) in the presence of sound fields. In addition, we fabricated a scaled-down ventilation model to examine the efficiency of particle filtration. Experimental results show that this technique significantly improves the removal efficiency, particularly for ultrafine particulates (0.3–1.0 μm). The maximum removal efficiency for $PM_{2.5}$ can reach 97.5 %, comparable to that of HEPA filters. The findings of this work demonstrate the effectiveness and controllability of this novel filter-less air purification method.

1. Introduction

Air pollution, which is closely linked to human activities and rapid urbanization, has emerged as a global concern. In areas with high-rise building clusters, the heat island effect resulting from urban sprawl has exacerbated environmental air pollution. Particulate matter (PM), a complex mixture of microscopic solid and/or liquid particles suspended in the air, is a significant contributor to this issue. Moreover, the COVID-19 pandemic has further heightened public awareness of indoor air quality. The diameters of PM typically range from a few nanometers to several hundred micrometers [1]. For example, the aerosol transmission of the severe acute respiratory syndrome coronavirus 2 (SARS-CoV-2) primarily involves particles in two size ranges: the sub-micron range (0.25–1.0 μm) and the super-micron range (>2.5 μm) [2,3]. Prolonged inhalation of PM can pose significant risks to both the respiratory and cardiovascular systems [4]. Furthermore, densely populated cities with limited land availability have seen a continuous rise in high-rise residential and commercial developments. The challenge lies in creating safe, comfortable, and efficient indoor environments that enhance the quality of life [5].

In office and commercial buildings, indoor air quality and thermal comfort, which are heavily reliant on heating, ventilation, and air conditioning (HVAC) systems, encounter more technical challenges compared to the outdoor environment [6]. Due to the functioning of mechanically ventilated systems, it is plausible that infectious viruses carried by airborne PM can be disseminated throughout buildings via the air recirculation of HVAC systems, leading to cross-region infections [7]. Although many filtering technologies have been identified, such as mechanical filtration, electrostatic precipitation, and ultraviolet germicidal irradiation (UVGI), have been proposed as defensive barriers against indoor airborne pollutants [8]. The electrostatic precipitator employs an electric field to ionize the gaseous medium, thereby

* Corresponding author at: Department of Civil and Environmental Engineering, The Hong Kong Polytechnic University, Hong Kong, PR China.
E-mail address: sk.lai@polyu.edu.hk (S.-K. Lai).

https://doi.org/10.1016/j.nanoen.2025.110674
Received 16 November 2024; Received in revised form 26 December 2024; Accepted 14 January 2025
Available online 15 January 2025
2211-2855/© 2025 Elsevier Ltd. All rights are reserved, including those for text and data mining, AI training, and similar technologies.

imparting a charge to the particulate matter, which facilitates their adsorption; this process is remarkably efficient; however, the generation of ozone remains a significant concern [9,10]. The UVGI technology can be a significant approach for inactivation but it is limited in particles removal, which makes it an effective conjunction instead of stand-alone technology [11]. Due to the limited space in the design of ventilation ducts, deploying fibrous-packed air filters (e.g., HEPA filter) with high removal efficiencies in ventilation ducts is a widespread practice. HEPA filters rely on several filtration mechanisms: diffusion, interception, and inertial impaction [12], which can be achieved by randomly arranged fiberglass materials. The performance is significantly influenced by their diameter, filter thickness, and face velocity. Generally, the minimum efficiency rating value (MERV) standard [13,14] is applied to low-grade filters used in mechanical ventilation ductwork. While HEPA filters are effective, they do require frequently regular maintenance and replacement as the filters can be clogged over time. HEPA filters can cause increased airflow resistance, necessitating greater reliance on HVAC fan power to overcome this resistance [15,16]. This can lead to longer system run-times and higher heating and cooling costs due to increased power consumption. Consequently, the development of smart filtering technology that is highly efficient, controllable, and requires minimal maintenance has become a key focus of research in the field of environmental pollution control [17]. Emerging techniques, such as acoustic-particle manipulation, are non-invasive methods for aerosol manipulation. Advancing engineering control technologies to efficiently filter indoor air pollutants and foster healthier living environments thus remains a critical concern.

Acoustic manipulation is a non-contact technique that uses sound waves to immobilize sub-micron particles in designated areas, making it easier to filter fine particles [18–20]. A theoretical investigation [21] examined microscale droplets under the mechanisms of acoustic and turbulent agglomeration. It demonstrated the phenomenon of rapid replenishment, which is attributed to the acoustic wake effects on small particles following orthokinetic collisions. More recently, ultrasonic acoustic agglomeration [22] has been examined as a pre-treatment mechanism for manipulating airborne particles through the addition of water droplets. An experimental study [23] explored the utilization of a resonant acoustic mixer to enhance agglomeration and collision process of dry powders. Additionally, an electro−acoustic coupling agglomeration technology [24] was used to enhance fire smoke elimination by using a high-voltage discharge device in conjunction with a sound source. Spraying droplets [25] were also utilized to couple with acoustic waves for cable fire smoke elimination. In our previous work [26], an acoustic trapping technique coupled with low-grade MERV filters was investigated, which significantly enhanced the filtration of sub-micron particles (0.3–1.0 μm) by 60−80 % when the sound intensity was reduced. However, the existing approach of exclusively applying acoustic-particle manipulation is inefficient and has the potential for further enhancement at fine and ultrafine particle levels. To maximize the utilization of acoustic power, a sound-driven triboelectric nanogenerator (TENG) system is being investigated to improve electrostatic precipitation for capturing fine particles.

Self-powering TENGs are cutting-edge devices capable of harvesting mechanical and ultrasonic energy [27–29]. Drawing inspiration from self-powering technology, TENGs function as air filters, improving the durability of charged filtration nanofiber membranes by allowing them to generate charges that attract and capture particles during filtration. Research is underway to develop new TENG designs aimed at optimizing surface friction, charge trapping, and discharge capacity [30–33]. In recent years, a variety of nanofibrous air filters have been developed because of the exceptional processability and flexibility of polymer materials [34,35]. Electrospinning is a low-cost method for preparing nanoscale polymer fiber structures [36]. Moreover, electrospun nanofibers can store charges to increase the electrostatic adsorption capacity of particles, which also improve the purification effects for bacteria and viruses [37]. He et al. [38] also developed highly air-permeable protective membranes through hierarchical nanofiber structuring, incorporating nanosized Ag-decorated BTO dielectrics to improve the electret effect and charge storage stability of the nanofibers. Additionally, rod-like ZnO nano-dielectrics were synthesized and integrated with PLA nanofibers [39], resulting in enhanced specific surface area, dielectric constant, and surface potential of the nanofibers, which contributed to improved performance in air filtration. Presently, electrified filtration membranes have shown significant potential to boost their electrostatic charges, thereby enhancing filtration performance for air purification. Liu et al. [40] developed a face mask with polyvinylidene fluoride (PVDF) electrospun nanofiber membranes to achieve electrostatic adsorption. Shao et al. [41] proposed a composite membrane that consists of polyvinyl chloride (PVC) and polyamide-6 (PA6) nanofibers, resulting in efficiency of 98.75 % and pressure drop of 67.5 Pa. Hu et al. [42] proposed a PVDF/UiO-66 composite nanofiber membrane for high removal efficiency. Nanoparticles were added into the polyetherimide (PEI) solution [43] to alter the properties of electrospun nanofibers, performing a filtration efficiency above 90 % with a pressure drop of 61 Pa. A comprehensive review and assessment of alternative mechanical-to-electrical energy harvesting polymers [44] were carried out, focusing specifically on non-fluoropolymer energy harvesters, including TENGs, ferroelectric elastomers, and flexoelectric polymers. The goal was to substitute traditional end-use fluoropolymers and tackle the pressing issue of environmental pollution. There are still practical challenges associated with using a single TENG for air purification. For example, the TENG filter requires a thick, multi-layered structure to achieve high filtration efficiency, but this design results in a significant pressure drop. Additionally, its application may be limited by factors such as dust holding capacity, the longevity of the nanofibers, and maintenance costs.

In this work, we introduce an innovative filterless “acoustic-driven TENG technique” to address issues in air purification. The proposed method simultaneously employs acoustic manipulation and electrostatic participation within ventilation ducts, creating a synergistic approach where the techniques complement and enhance each other. A U-shaped resonating design is developed to generate a standing wave sound field, while contact-separation TENGs produce electrical voltage in response to the sound pressure field. Fibrous-type TENGs, made from electrospun nanofibers, offer the benefits of nanoscale diameters and a high surface area-to-volume ratio. The stretching fabrication method ensures a significant draw ratio, high molecular alignment, and minimal defects in the nanofibers [45,46]. The use of PVDF nanofibers produced through the electrospinning process results in nanofibers with a high β phase fraction and crystallinity, achieved by aligning molecular dipoles (–CH2 and –CF2) along the direction of the applied voltage [47,48]. This configuration can enhance their flexibility and air permeability, making them particularly suitable for filtering applications. Our proposed design is capable of functioning in two air filtration scenarios: passive and active PM removal. In the passive state, with acoustic wave stimulation, fibrous-type TENGs can generate a certain level of electrical voltage through airflow-induced contact-separation and can capture fine particles using traditional mechanisms such as interception, impaction, and diffusion, without any additional requirements. Additionally, active filtration can be achieved in two stages: (i) particle interaction driven by acoustic waves, created by a standing wave field within U-shaped acoustic resonators, and (ii) a high-voltage electrostatic field generated by TENGs, powered by acoustic energy. It is recognized that most airborne particles possess either a net negative or positive charge [49]. The electrostatic capture mechanism further enhances the capacity to hold ultrafine particles. This work is organized as follows: Section 2 describes the fabrication of the TENG unit, the working principle of the proposed filtering system, and the experimental setup. Section 3 presents the results on the electrical and filtration performance of the proposed system under sound stimulation, including parametric studies, significant tests, and a comprehensive comparison with existing filters. Section 4 summarizes the key findings of this study.

2. Working principle and experimental setup

2.1. Fabrication of TENG units

PVDF powder (*Arkema Kynar 761*, *Mw~44,000 g/mol*) and N,N-Dimethylformamide (DMF) were utilized to fabricate electrospun nanofiber thin films. The PVDF powder, with a mass fraction of 18 %, was dissolved in the DMF solvent. The electrospinning process was carried out at 18 kV, with a 15 cm gap between the needle tip and a grounded rotating drum collector. To enable the connection between the TENG unit and the ventilation tube, a rectangular acrylic frame was used. The acrylic was cut into a shape that served as the structural framework for the TENG unit, measuring 90 mm by 90 mm. A 15-μm-thick Kapton thin film was prepared as a spacer to separate the triboelectric positive and negative layers. A triboelectric layer was created by affixing a conductive fabric, a Kapton layer, and a PVDF electrospun nanofiber thin film to one side of the acrylic frame, resulting in a sandwich structure. A traditional nonwoven fabric air filter (polypropylene), a synthetic air filter sponge (polyurethane foam), and a conductive fabric (metallic fibers) were each utilized as additional triboelectric layers. These layers were combined with the triboelectric layer containing an electrospun nanofiber thin film to create different TENG units. Table 1 presents detailed information on various TENGs used for experimental testing.

2.2. Working principle

The schematic of the TENG structure used for air purification is shown in Fig. 1(a). The fiber-type TENG allows contaminated airflow containing dust, particulate matter, and other substances to pass through. With nanoscale diameters and sufficient gaps between the nanofibers, PM can be obstructed within the mesh structure through a passive mechanism and captured by the electrostatic precipitation effect stimulated by periodic sound waves. We used a TENG unit composed of layers of nanofiber thin film and nonwoven fabric to explain the working principle under sound effect, as shown in Fig. 1(b). This process is divided into four stages:

(I) The two triboelectric layers make contact and rub against one another. As a result of the frictional electrification effect, surface charges are rapidly transferred between the two materials. The PVDF nanofiber thin film, which has a strong inclination to gain electrons, becomes negatively charged, while the fabric layer tends to become positively charged. It is important to note that electron transfer is not the only mechanism contributing to the phenomenon of polymer–polymer contact electrification, a subject that remains a significant focus of ongoing academic discussion [50–53].

Table 1
Descriptions of various TENG units adopted in the proposed filtering system.

Sample no.	Description
TENG-S0	Tribo-negative layer: PVDF electrospun nanofiber thinfilm Tribo-positive layer: Conductive fabric (metallic fiber)
TENG-S1	Tribo-negative layer: Synthetic filter sponge (polyurethane foam, 15 ppi, 5 mm in depth) Tribo-positive layer: PVDF electrospun nanofiber thinfilm
TENG-S2	Tribo-negative layer: Synthetic filter sponge (polyurethane foam, 45 ppi, 5 mm in depth) Tribo-positive layer: PVDF electrospun nanofiber thinfilm
TENG-S3	Tribo-negative layer: PVDF electrospun nanofiber thinfilm Tribo-positive layer: Nonwoven fabric fiber (polypropylene product, less than 1 mm in depth)

Note: The descriptions within parentheses indicate the primary components of the substance.

(II) In the second stage, as the PVDF nanofiber thin film detaches from the fabric material, a voltage difference is created between the two electrodes. An oscilloscope was used to measure the open-circuit voltage.
(III) As the separation distance reaches its peak, an equilibrium state is attained, resulting in the highest open circuit voltage.
(IV) In the final stage, as the two triboelectric layers move closer together, the open-circuit voltage decreases correspondingly. Throughout the ongoing contact-separation process, high voltage spikes occur periodically.

Experimental studies were conducted in this work to demonstrate the overall performance of the proposed filtering system. Fig. 1(c) depicts a top view of the schematic diagram of the ventilation duct used for the filtering test. The particles within the airflow appeared to align with the flow fields. In the particle release area, aerosols were generated and released at the flow inlet. In the acoustic active region, the loudspeakers were represented as two rectangles positioned opposite each other on the side walls of the resonating chambers. In the measurement area, a sensor probe and a particle counter were employed to monitor variations in flow rate and particle concentration. An extraction fan was used, and the released particles were filtered through a HEPA filter to eliminate any interfering factors. A U-shaped configuration has been investigated in our previous work [26], which included confined resonant chambers to facilitate particle trapping. The acoustic waves emitted from loudspeakers were in the opposite direction against the incoming airflow to enhance the efficiency of acoustic treatment. A one-dimensional standing wave field can be established to generate acoustic pressure nodes. The emitted sound waves were confined and reflected by the hard boundary walls of the chamber. At this point, the contact-separation TENG units were placed at the center of the resonant chambers, aligning with the pressure node of the fundamental resonant frequency in the U-shaped acoustic resonators. Previous studies have indicated that using a fundamental frequency can enhance particle reduction. To avoid any impact of the TENGs on the flow field within the U-shaped resonating chambers when increasing the operating frequency, the TENGs were kept at the center of the resonating chambers.

Consider the present design as a closed tube, the resonant frequency can be calculated as follows [54]:

$$f = \frac{mc}{2L}, \quad m = 1, 2, 3, \cdots \tag{1}$$

where f is the frequency in Hz, c is the speed of sound in air (~343 m/s), L is the length of the resonant chamber, and m is the harmonic order number of the emitted frequency. In this study, the acoustic pressure model is simplified as a two-dimensional acoustic enclosure driven at a constant frequency and same phase. Indeed, sound frequencies are affected by the geometric properties of the chamber's length. In this study, the chamber length is approximately 215 mm, which leads to a theoretical fundamental frequency of about 798 Hz, as determined by Eq. (1). Subsequently, an experimental fine-tuning test was performed to investigate the operating fundamental frequency within the range of 750–850 Hz. The filtration performance was optimal at a frequency of 795 Hz, likely reflecting the actual experimental conditions. Therefore, this frequency is designated as the fundamental frequency, while the second and third resonant frequencies are 1590 Hz and 2385 Hz, respectively.

To assess the impact of acoustic intensity, we define the sound pressure level (SPL) using the following standard logarithmic form:

$$SPL = 20\log_{10}\left(\frac{p}{p_0}\right)(\mathrm{dB}) \tag{2}$$

where p is the root-mean-square acoustic pressure, and p_0 is the reference sound pressure (20×10^{-6} Pa).

Fig. 1(d) and (e) illustrate the schematics of the acoustic active zone

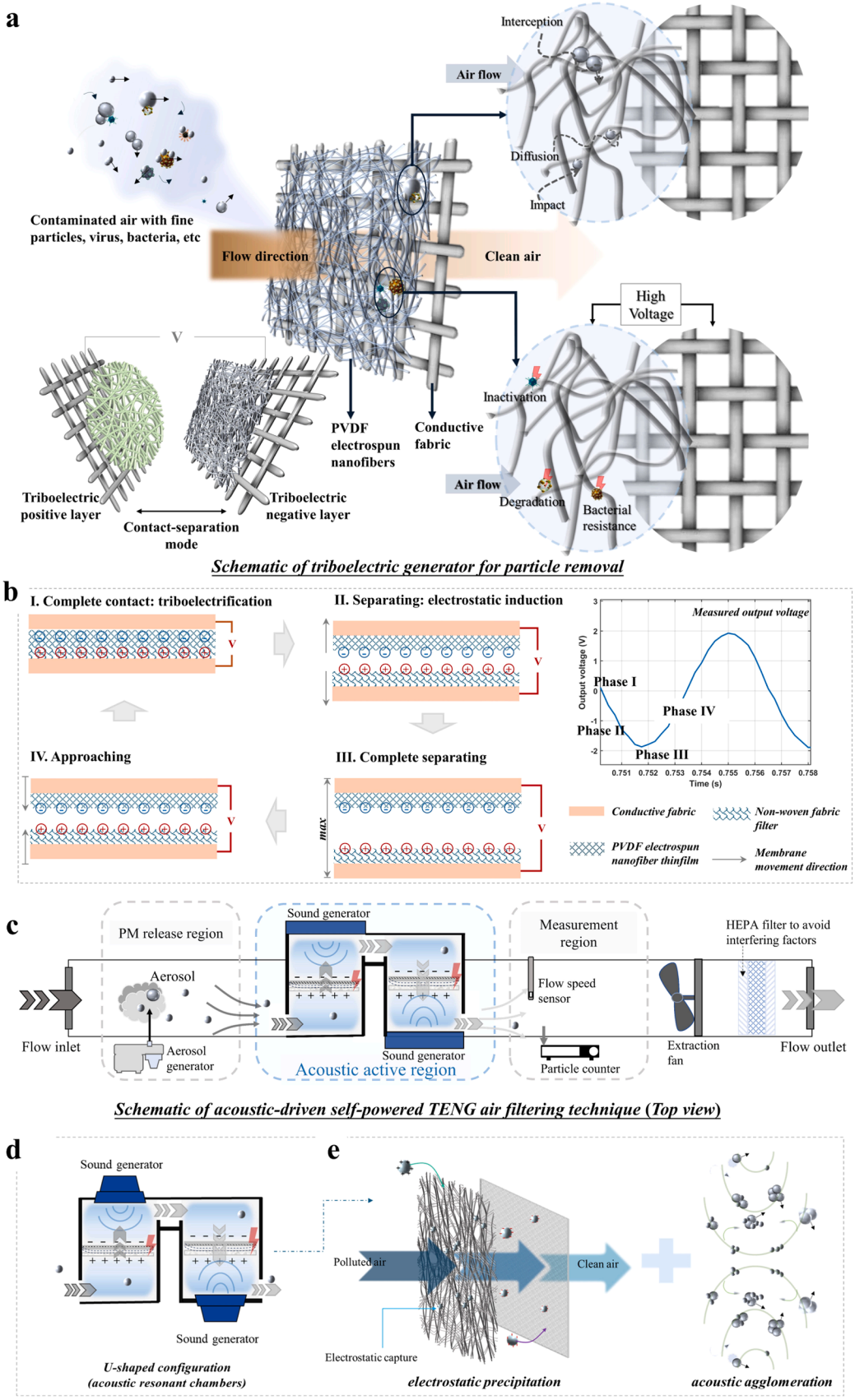

Fig. 1. Illustration of the working mechanism: (a) a schematic representation of the TENG and its air filtering mechanism; (b) the working mechanism of the TENG under acoustic excitation; (c) a top-view schematic diagram of an acoustic-driven TENG air filtering system in a ventilation duct; (d) and (e) schematics of the acoustic active zone formed by a U-shaped configuration with attached TENGs to facilitate acoustic-driven particle agglomeration and electrostatic precipitation.

(specifically, the U-shaped resonating design) and the locations of TENGs installed within the resonant chambers. In our previous work [26], we performed a numerical analysis using COMSOL Multiphysics® software to investigate the sound pressure field within the U-shaped configuration and the dynamic motion of particles under sound effect. The contour plot of sound pressure illustrated the locations of pressure nodes and anti-nodes [26], leading to a peak pressure differential in the central region of the resonant chambers at the fundamental frequency. In this region, the particles tended to accumulate under the standing wave field. This phenomenon was demonstrated through a wood-powder test [26] where powders were forced and aligned into a uniform multi-line pattern with regular intervals between the lines. Standing wave fields can cause particles to accumulate near the pressure node region, enhancing particle interactions. At the same time, periodic acoustic waves can continuously energize the triboelectric layers, creating an electrostatic precipitation effect. The TENG units placed within the acoustic resonating chambers can harness the acoustic waves for high voltage generation and demonstrate an increased ability to capture particles stimulated by the acoustic waves. This results in a more efficient particle-trapping capability for the acoustic-driven TENG filtering system.

2.3. Experimental setup

To examine the synergistic effects of particle removal in a U-shaped design configuration, a scaled-down model of a ventilation duct with a filtering system was constructed using acrylic materials. The cross-sectional dimensions of the scaled-down tube were 10 cm by 10 cm (width and height). Two acoustic resonant chambers were fabricated by partitioning a cubic transparent acrylic material into two rectangular parts. Two circular apertures were excised from the tube walls within the resonant chambers, and two loudspeakers (*TANBX, TB-412, 4-in, coaxial audio loudspeaker*) were deployed into the circular holes. Two acrylic plates, each with a thickness of 10 mm, were positioned as reflectors in the opposite direction of the loudspeakers. Instead of using fully enclosed acoustic resonant chambers, the side walls of the proposed resonant chambers were designed with circular openings to permit airflow, with each opening having an area of 176.7 mm^2. It is noted that the loudspeakers were operated at the same frequency. By incorporating an interior wall between the two resonance chambers, interference effects can be minimized and ignored. Additionally, blu-tack reusable adhesive was used to seal the gaps in the acoustic resonant chambers to minimize sound leakage during the experiments.

A scaled-down experimental prototype was constructed to investigate filtration performance under different airflow conditions, as depicted in Fig. 2. Aerosol particles were generated using an aerosol generator (*Model 8026, TSI Incorporated, USA*) with a sodium chloride (*NaCl*) solution and released at the flow inlet. The particles then entered the designed filtration system to undergo the trapping process. The filtering performance was evaluated using a particle size counter (*Model BT-620, MetOne Instruments Inc., USA*). This particle counter was equipped with an integrated aspirator pump to control the flow rate during measurements. Once activated, both the aspirator pump and the particle size analyzer can operate continuously. The particle concentration data was recorded at a rate of one measurement every two seconds, providing an average concentration based on the air volume extracted during that period. To reduce turbulence fluctuations and minimize data bias, particle concentration was measured over a duration of 5 minutes for each individual variable change. An airflow profile was induced by an extraction fan (*Type 110/100, diameter 100 mm, 3600 r/min, 110 m^3/h*) mounted at the end of the ventilation tube with an adjustable control circuit for flow rate control. A hot-wire anemometer wireless smart probe (*Model 405i, Testo Inc., USA*) was inserted into the duct (~5 cm of insertion depth) to monitor the environment in the ventilation duct, e.g., temperature, flow rate, and flow velocity. The pressure drops (Δp) between the inlet and outlet of the

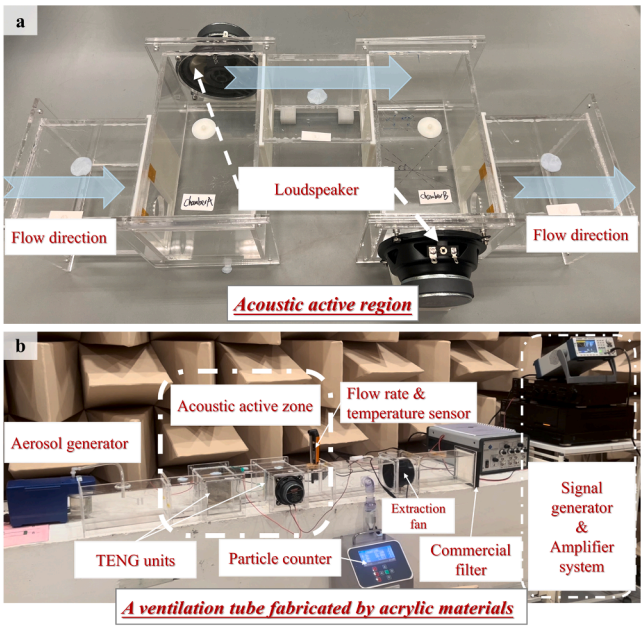

Fig. 2. A scaled-down experimental setup: (a) an enlarged view of the acoustic active region; and (b) an entire view of the ventilation duct.

acoustic active zone were measured by a micromanometer (*Fluke-922/Kit, Fluke International Corporation, USA*). To optimize filtration efficiency, we examined the operating frequency (in Hz) of loudspeakers, the applied SPL (in dB), and the air flow rate in the duct under the distribution of various particle sizes (i.e., 0.3 −4.0 μm). The removal coefficient that indicates the filtration efficiency (α) of the filtering system is defined by [54–56]:

$$\alpha(\%) = 1 - \frac{N_o}{N_i} \tag{3}$$

where the number of particles at the inlet is N_i and at the outlet is N_o. The quality factor (QF) can be derived to describe the overall performance of the filtering system as follows [55]:

$$QF(\mathrm{Pa}^{-1}) = -\frac{\ln(1-\alpha)}{\Delta p} \tag{4}$$

where $\Delta p = P_{out} - P_{in}$ is the pressure drop between the flow inlet and flow outlet of the filtering system, in which P_{out} and P_{in} are the outlet pressure and inlet pressure, respectively.

3. Results and discussion

3.1. Electrical and dynamic performance of TENG units under acoustic waves

To characterize the electrical signals generated during the triboelectric process, TENGs were fabricated and positioned at the central locations of acoustic resonant chambers for measurement, aligning it with the pressure node of the fundamental frequency in the acoustic resonator. Four types of TENG samples (i.e., TENG-S0, TENG-S1, TENG-S2, and TENG-S3) were prepared and tested in filtration experiments. Significant differences in electrical output performance were observed due to variations in the materials used.

Fig. 3 depicts the morphological features of several materials employed as triboelectric layers. The picture of the prepared triboelectric layers is presented in Fig. 3(a). To show the morphological structure of the materials, SEM images of nonwoven fabric fibers, PVDF nanofibers, conductive fabric, and synthetic filter sponges, respectively, are presented in Fig. 3(b)−(f). The diameter distribution was measured and

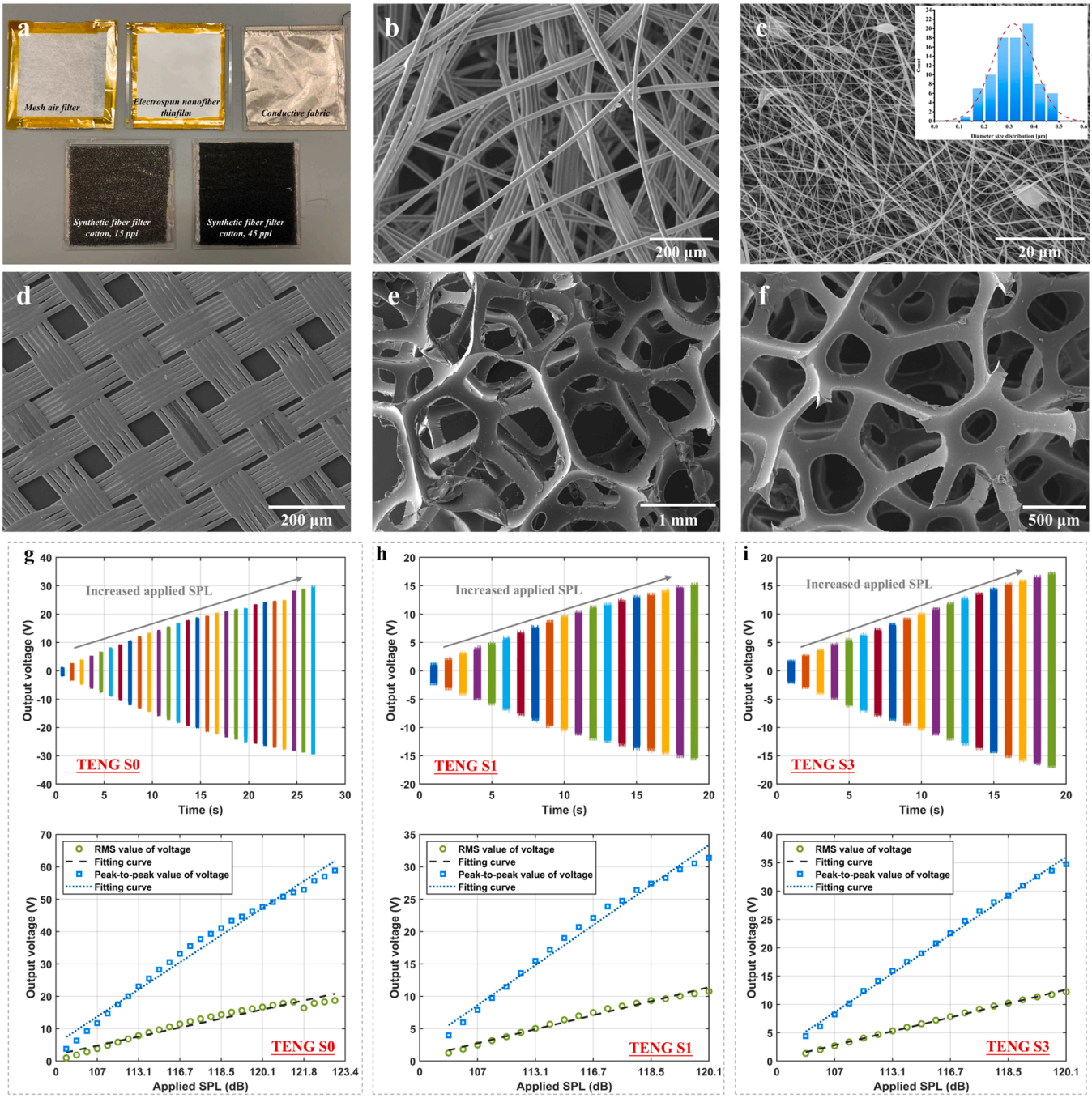

Fig. 3. Electrical outputs of TENG units under acoustic excitation in the resonant chambers: (a) Photographs of triboelectric layers used in the experiment; (b) SEM images of nonwoven fabric filter; (c) SEM images of PVDF electrospun nanofibers, with a measured mean diameter of approximately 0.3 μm; (d) SEM images of conductive fabric; (e) and (f) SEM images of different types of synthetic fiber filter foams with porosities of 15 pores per inch and 45 pores per inch, respectively; (g)–(i) the output peak-to-peak voltages of various TENG units measured by an oscilloscope in time domain (the applied SPL increased from 104 dB to 123 dB with time varying) and the associated effective voltage of various TENG units (i.e., TENG-S0, TENG-S1, and TENG-S3, respectively).

presented (*Nano Measurer Version 1.2*). It can be observed that the nonwoven fabric fibers and PVDF electrospun nanofibers were randomly interwoven and layered, creating a mesh structure with numerous tiny pores. The nanofibers had significantly smaller diameters compared to the nonwoven fabric fibers, with most of them ranging from 100 nm to 500 nm. With the advantages of one-dimensional nanostructured morphology, nanofibrous materials possess better response properties to bulk materials [34,57], thereby facilitating a superior electrostatic effect under sound stimulation. The small diameter of nanofibers can enhance the performance of TENGs by improving carrier mobility due to their larger specific surface area and higher surface-to-volume ratio, resulting in a quicker response to external stimuli. When periodically excited by a sound field, the tribo-negative and tribo-positive layers continuously contacted and rubbed against each other. This frictional electrification effect transferred surface charges between the two layers. A benchmark research [58] provided a quantitative ranking of the triboelectric series and compared their triboelectric charge densities. For TENG-S0 and TENG-S3, the PVDF material exhibited high electron affinity, while the conductive fabric/nonwoven fabric layers tended to lose electrons. As a result, the nanofiber thin films became negatively charged, whereas the

other layers acquired a positive charge. In the case of TENG-S1 and TENG-S2, the primary component of the synthetic filter sponge was polyurethane, which tended to gain electrons, causing the nanofiber thin films to lose electrons in this scenario.

Fig. 3(g)−(i) display the open-circuit voltages of the TENG units (i.e., TENG-S0, TENG-S1, and TENG-S3) in response to sound stimulation, along with the corresponding peak-to-peak and effective voltages. An oscilloscope was used to measure the output voltage of the different TENGs. As time progressed, the applied SPL increased accordingly. Specifically, TENG-S0 achieved a peak-to-peak voltage (V_{pp}) of ~61 V when an input power of approximately 1.4 V was supplied, as recorded by the signal generator. The output voltages, including both peak-to-peak and RMS values, exhibited a linear and consistent relationship with the supplied input power. TENG-S3 exhibited a greater electrical output compared to TENG-S1, whereas TENG-S0 demonstrated even higher outputs compared to TENG-S1 and TENG-S3. This is attributed to the varying electrical properties resulting from tribo-polarized charging. It is well-known that metals have a greater tendency to lose electrons, whereas dielectric materials tend to gain them. Hence, metal-on-dielectric configuration is considered one of primary forms of TENGs for producing a significant voltage. Previous research [58] examined the triboelectric charge densities through a standardized experimental investigation. The triboelectric charge densities of several materials, such as abrasion-resistant polyurethane (PU) rubber, polyvinylidene fluoride (PVDF), and polypropylene (PP), are around –110 μC/m^2, –90 μC/m^2, and –30 μC/m^2, respectively. When two materials that have a greater difference in triboelectric charge density are rubbed together, they enable to create a more powerful electrostatic effect. In this regard, the disparity between PVDF and polyurethane is less than that between PVDF and polypropylene, resulting in a relatively low electrical output of TENG-S1.

To examine the displacement of TENG when exposed to an acoustic standing wave field, we placed the TENG-S0 into the acoustic resonant chamber and utilized a laser displacement sensor (*LK-G405 & LK-G3001 series, Keyence Cooperation, USA*) to observe and acquire the displacement data, as shown in Fig. 4(a). Fig. 4(b) displays the raw time-domain signal, while Fig. 4(c) demonstrates the mean and standard deviation of the measurement under various applied SPLs. It can be inferred that the TENG exhibited self-vibration and showed a slight tendency to move forward in the direction of acoustic wave, as indicated by the increase in the mean value. This can be interpreted as the effect of sound waves generated by the loudspeaker. The parametric features of the time-domain data are presented in Table 2, including the mean value, standard deviation, peak value, effective value, skewness, kurtosis, and crest factor. It is noted that the unit of displacement is millimeter. As the applied SPLs increase, the kurtosis also increases, indicating a rise in the vibrating amplitude of the TENG. Standardization, as a commonly used data pre-processing method [59], was performed to eliminate the offset impact between datasets. The provided information relates to crest factors, defined as the ratio between the maximum value and the effective value, indicating the peak value of the signal in the waveform. The crest factors exhibit a consistent trend with increasing applied SPLs, indicating that the TENG is subjected to greater sonic impact during this process.

3.2. Filtration performance of the U-shaped filtering system

The effort to create an air filtering system that is both highly efficient

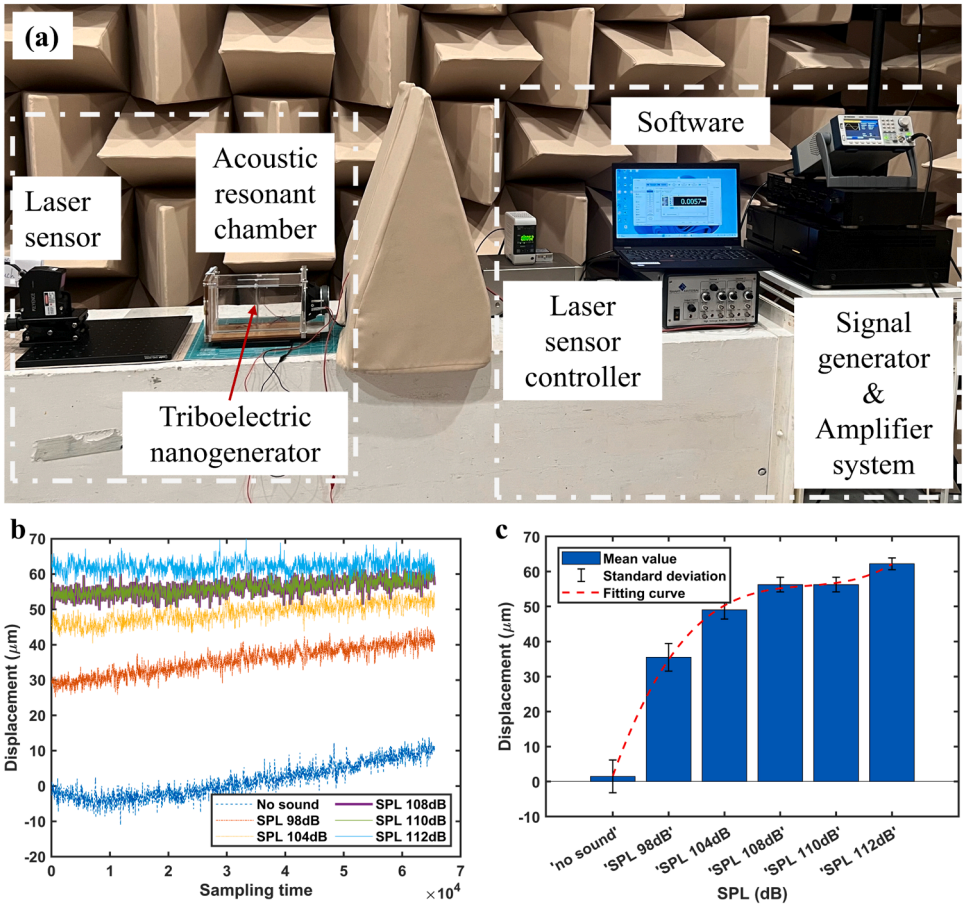

Fig. 4. Displacement variations of the TENG unit inside the acoustic resonant chamber under different applied SPLs: (a) measurement setup; (b) raw time-domain measurement data ranging from 98 to 112 dB; and (c) comparison of the mean displacement values under various SPLs.

Table 2
Parametric characteristics of measurement data for the displacement of TENG unit excited by standing acoustic waves in the resonant chamber.

SPL	Mean	Standard deviation	Peak	RMS	Skewness	Kurtosis	Crest factor*
			Raw data				Standardized data
No Sound	1.4640	4.6962	13.9000	4.9191	0.3549	2.0820	2.6481
98 dB	35.4879	3.9454	45.2000	35.7065	−0.1402	2.0440	2.4617
104 dB	49.0469	2.6620	56.3000	49.1191	−0.1573	2.3191	2.7246
108 dB	56.2471	2.1009	63.2000	56.2863	0.1286	2.7370	3.3094
112 dB	62.1819	1.6820	70.0000	62.2046	0.0999	3.3789	4.6482

* The crest factor is calculated by using the standardized data of the peak and rms values. The measurement unit is in millimeters.

and low in resistance has faced several challenges. In this section, an experimental prototype featuring a U-shaped design with an acoustic-driven TENG filtering system was developed and constructed to evaluate its filtration performance by measuring PM concentration. The filtration of aerosol particles of specific sizes was optimized to validate the proposed parameters and boundary conditions. To assess the effectiveness of the proposed filtering system, we systematically evaluated the device's performance in terms of PM concentration reduction and removal coefficient, thereby determining its filtration efficiency. Case studies were conducted in three different scenarios:

(i) the application of acoustic waves in the U-shaped configuration for particle trapping (sound treatment for PM removal);
(ii) the inclusion of TENGs in the U-shaped configuration for particle filtering (passive-type PM removal); and
(iii) the use of acoustic waves to perform acoustic-particle manipulation and activate TENGs in the U-shaped configuration (combining acoustic agglomeration and electrostatic precipitation for PM removal).

In addition, a statistical significance study (i.e., a two-tailed t-test) was performed to demonstrate the differences in experimental tests with and without air filtering treatments.

Fig. 5 presents the particle concentration results for particle sizes ranging from 0.3 μm to 4.0 μm. The experimental test compared groups with and without sound treatments applied in the U-shaped configuration, excluding the involvement of TENGs in this scenario. The control group, represented by the blue-violet bars, shows particle concentration without sound treatment. The particle concentration with sound treatment, ranging from 114 dB to 122 dB, is depicted by the other bars. The application of sound treatment significantly reduced PM levels. As the SPL increased, the presence of acoustic waves led to a nearly linear decrease in PM concentration, particularly for fine particles in the range of 0.3−0.8 μm. These results indicate that acoustic waves have a noticeable impact on particle trapping within the U-shaped configuration, restricting the mobility of ultra-fine particles and preventing them from being easily carried downstream by the airflow in the ventilation duct.

Fine particles within the U-shaped configuration are more likely to experience collision, adhesion, and sedimentation under acoustic stimulation. A sampling method [60,61] was utilized to collect particle precipitation via an array of circular aluminum tapes (diameter = 10 mm) placed at the bottom of the U-shaped duct. A sample holder was prepared via 3D printing technique, as shown in Fig. 5(g). These tapes were thoroughly cleaned with isopropyl alcohol and deionized water. As shown in Fig. 5(h), no observable particles can be seen on the surface of the aluminum tapes, which represents the tapes with completely cleaning and no treatment on it. The prepared samples were stored in petri dish with parafilm. Fig. 5(h)−(k) show the morphological features of particle precipitations in the U-shaped duct with and without acoustic waves. Fig. 5(i) illustrates particle precipitation when NaCl aerosol was introduced into the acoustic resonant chamber for one hour. Some particles can be seen settling at the bottom of the resonant chamber due to gravity. These particles were measured approximately to be 10 μm in length and 2.9 μm in width. Fig. 5(j) shows particle precipitation after one hour of sound treatment in the acoustic resonant chamber. A distinct multi-line pattern of particle sedimentation and stripe-shaped particle clusters can be clearly observed on the surface of the aluminum tapes. The sediments form a neatly distributed line pattern, with stripe-sedimentation particles ranging from approximately 26.6 μm (shorter lines) to 48.2 μm (longer lines) in length. The particle clusters were measured around 104.1 μm in length and 17.5 μm in width, significantly larger than the particles in Fig. 5(i). This demonstrates that sound treatment has a substantial effect on particle collision, causing them to coalesce and eventually settle at the bottom. Additionally, the planar morphology of the sediments was revealed by switching the SEM scanning to backscattered electrons (BSE) mode, as shown in Fig. 5(k).

Next, we characterized an air filtering system that incorporated U-shaped acoustic resonant chambers and two TENGs. Fig. 6 shows the particle concentration for sizes ranging from 0.3 μm to 4.0 μm. The control group, represented by the dark-blue bars, indicates sampling data without any sound treatment or passive-type TENGs. The other bars display the results of two different filtering treatments: (i) using passive-type TENGs as air filters in the U-shaped configuration without sound stimulation, and (ii) applying sound waves to promote acoustic agglomeration while simultaneously stimulating TENGs for electrostatic precipitation in the U-shaped configuration. The applied acoustic power (measured by sound pressure level SPL) ranged from 104 dB to 123 dB. It is evident that the acoustic-driven TENG treatment significantly reduced particle concentrations, with the effectiveness increasing with SPL. The applied sound frequency was 795 Hz.

A two-tailed *t*-test, also referred to as independent samples *t*-test, is a statistical procedure utilized to compare the means of two independent sample groups to ascertain whether a significant difference exists between them. It was conducted in this work to analyze the PM concentration data collected under various conditions to identify whether the differences in filtering efficiency were statistically significant, as shown in Fig. 7. A paired-group *t*-test was used to compare the mean outcomes of the four groups: "no treatment", "sound treatment", "TENG-based air filter", and "combined TENG-based filter with sound treatment". The control group represents the particle concentration without any treatment in the U-shaped configuration. The treated groups include: (i) particle concentration with sound treatment in the U-shaped configuration at an SPL of 104 dB, (ii) particle concentration with passive-type TENG air filtering in the U-shaped configuration, and (iii) particle concentration with TENGs subjected to sound stimulation at an SPL of 104 dB. According to Fig. 7, the data analysis revealed significant statistical differences between the treatment and control groups. The test produced a *t*-statistic with a corresponding *p*-value much less than 0.01. The symbol "*** " in Fig. 7 indicates $p < 0.01$, signifying strong significance. Therefore, there are statistically significant differences between the treatment and control groups. This provides compelling evidence that the proposed filtering system has a substantial impact on PM removal. Fig. 8 shows the removal coefficients (Eq. (3)) for passive-type TENG-S3 and TENG-S3 subjected to sound stimulation in the U-shaped design for particle sizes ranging from 0.3 to 3.0 μm. The peak removal coefficient reaches 97.5 % for $PM_{2.5}$ with TENG-S3 subjected to an SPL of 123 dB in the resonant chambers.

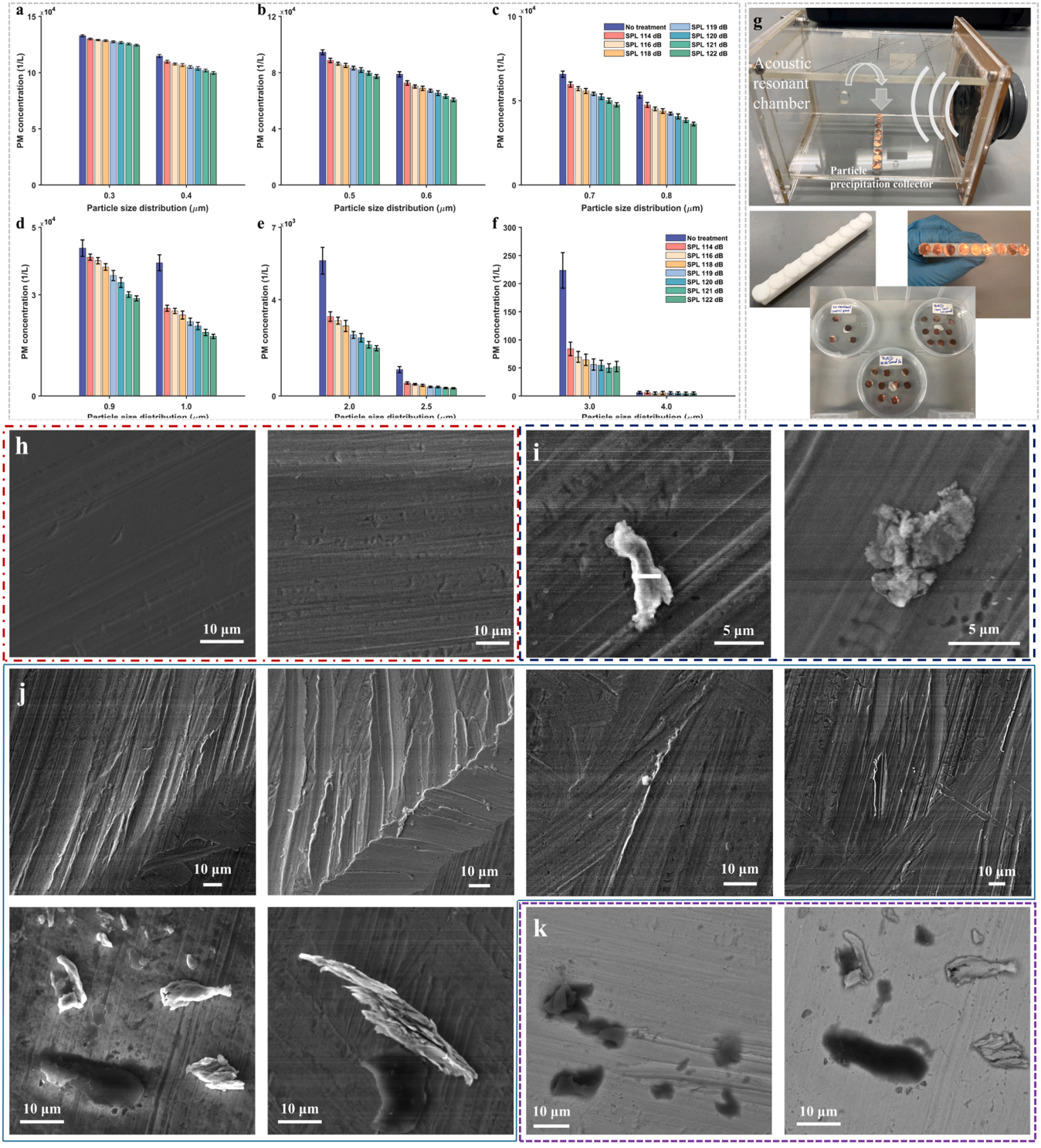

Fig. 5. Particle number concentrations under various 114 –122 dB in the U-shaped configuration: (a)–(d) fine particles (0.3–1.0 μm); (e)–(f) coarse particles (2.0–4.0 μm). The legends of "*no treatment*" and "*SPL*" represents different scenarios without and with sound treatments within the U-shaped configuration; (g) sample preparation for SEM experiment; (h)–(k) SEM images of particles precipitation scanning via secondary electrons (SE) signal; and (j) Particle precipitation scanning via backscattered electrons (BSE) signal. It is noted that the particle precipitation was collected via copper film attached on the bottom of the acoustic resonant chamber. The copper film was cleaned completely with isopropyl alcohol and deionized water and stored in the sealed petri dishes before experiments.

3.3. Parametric analysis of the U-shaped filtering system

In addition to studying the filtration efficiency, we performed a parametric investigation of the proposed filtering system under various operating scenarios. Three case studies were also conducted to explore the dependence of the device performance with various types of TENGs, sound frequencies, and airflow rates. These parameters are the critical variables that affect the effectiveness of the current filtering system. This section offers a comprehensive discussion on the air purification effectiveness of the proposed system.

To illustrate the influence of various types of TENG filters on the efficacy of filtration, we examined three different TENGs (i.e., TENG-S1,

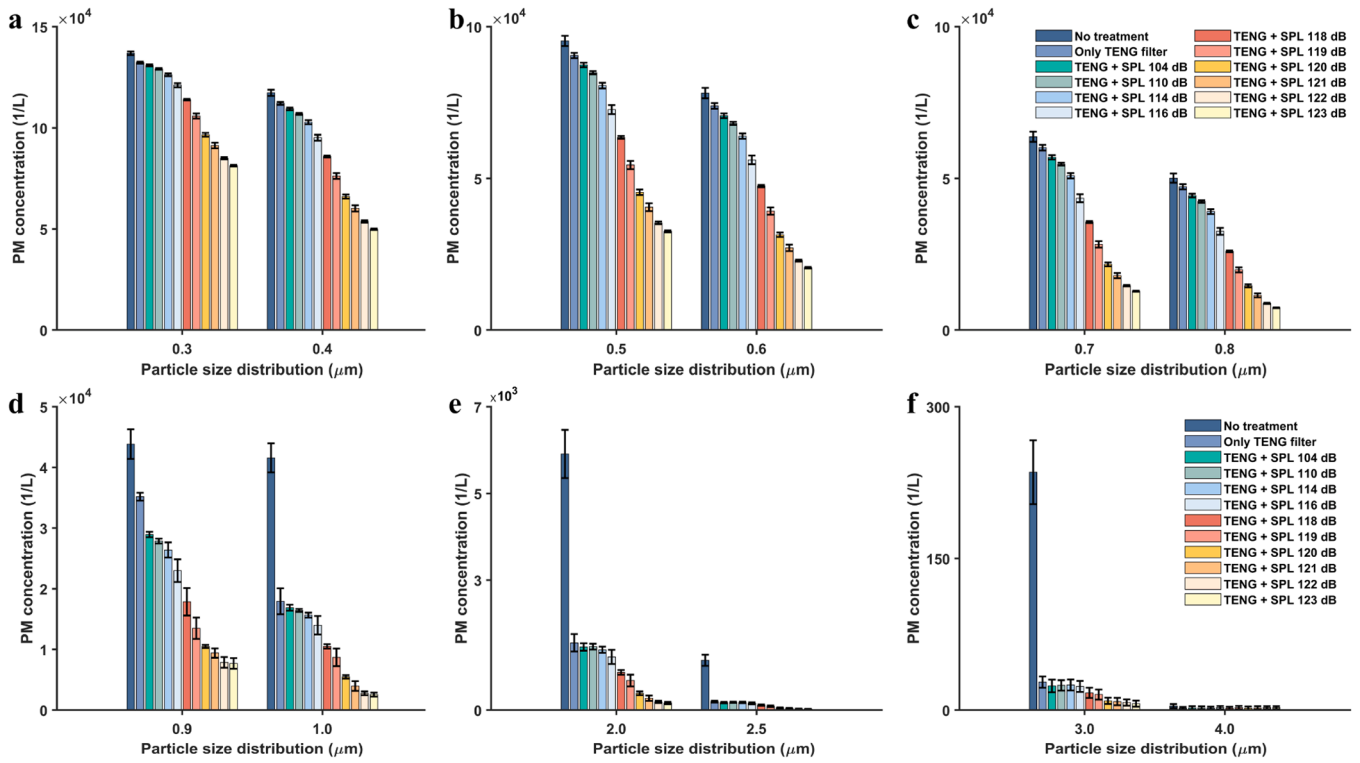

Fig. 6. Particle number concentrations under 114–122 dB with TENGs in the U-shaped configuration: (a)–(d) fine particles (0.3–1.0 μm); and (e)–(f) coarse particles (2.0–4.0 μm). The legends of "*No treatment*", "*only TENG filter*", and "*TENG+SPL*" represents different examined scenarios, i.e., no sound or TENGs in the U-shaped configuration, with TENGs as membrane filters in the U-shaped configuration, and with TENGs and applied sound waves in the U-shaped configuration.

TENG-S2, and TENG-S3) and affixed them within the acoustic resonant chambers for experimentation. Fig. 9 presents a comparison of PM removal coefficients with different TENG filters in the U-shaped configuration. The applied SPL was 119 dB, 120 dB, and 121 dB, as shown in Fig. 9(a)–(c), respectively. The dashed lines depict the filtration efficiency of TENGs as a passive-type filter in the U-shaped configuration, while the dash-pot line illustrates the filtration efficiency under acoustic effect without TENGs. The application of acoustic waves significantly enhanced the filtering effectiveness compared to passive-type TENGs, especially at the fine particle range (0.3–0.8 μm). For example, the filtration coefficient shows improvement from 2.3 % to 22.6 % at $PM_{0.3}$, and it increases from 5 % to 60 % at $PM_{0.8}$ with SPL in 119 dB (Fig. 9(a)). For coarse particles, the impact of acoustic waves was also significant. The effectiveness increased from 65 % to 79.8 % at $PM_{1.0}$. The improvement in filtration efficacy due to acoustic effects is illustrated by the blue, yellow, and orange shaded areas in Fig. 9. The maximum removal coefficient reached 96.9 % for $PM_{2.5}$ with a TENG-S3 filter at an SPL of 121 dB. It is important to note that in these experiements the acoustic frequency was set at 795 Hz. When the TENG-S1 and TENG-S2 systems were not excited by sound, their removal coefficients were found to be less than 40 % across the tested particle size distributions. However, with the application of acoustic waves, the filtering performance improved significantly. For example, the removal coefficient increased to approximately 60 % for $PM_{0.9}$ at an SPL of 121 dB, with a maximum reaching 80 % for $PM_{2.5}$ (as indicated by the red and yellow lines). Under the same power conditions, the effect of acoustic wave excitation varied between the TENG-S1/TENG-S2 filters and the TENG-S3 filters. This difference is likely due to the larger pore diameters of the TENG-S1/TENG-S2 filters, which are about 2–3 mm (see Fig. 3). The larger pore diameter may result in less effective control of fine and ultrafine particles within the internal porous structures of TENG-S1/TENG-S2, even when they are periodically charged by the contact-separated electrostatic effect under acoustic excitation.

A comparison of the filtering efficiencies at different resonant frequencies is presented in Fig. 10, comparing particle concentration at the first three resonant frequencies, i.e., $f_1 = 795$ Hz, $f_2 = 1590$ Hz, and $f_3 = 2385$ Hz. The acoustic power ranged between 118 and 120 dB, as shown in Fig. 10(a)–(c). During the adjustments of the acoustic frequency, we kept the TENG positioned at the center of the acoustic resonating chamber to ensure a single measurement variable was controlled in the experiment. Fig. 10(d) presents a simple illustration for the pressure variation of standing wave fields at the first three frequency modes. The removal coefficients raised dramatically under the fundamental frequency, indicating a strong recorded trapping effect (green dashed lines). At 2385 Hz, the removal coefficient can be improved at fine particle size distribution (0.3–1.0 μm), but limited enhancement at coarse particle size distribution (above 1.0 μm) had resulted. In comparison to the fundamental frequency, higher order harmonics of sound waves are likely to dissipate energy faster. Referring to our previous work [62], the contour plots of sound pressure fields revealed that higher sound frequencies resulted in more dispersed and narrower zones of acoustic wave focusing. In general, the acoustic waves induce a significant reduction in particle concentration, especially at fine particle size distribution. As their small mass, fine particles tend to be easier manipulated under acoustic-driven stream within the resonant chambers. In comparison to their smaller counterparts, larger particles are less affected by sound waves directly due to the greater inertia. Aggregates may be formed when these smaller particles collide with and adhere to the larger particles, closely following the motion of sound waves [63]. This may explain the enhanced filtration efficiency observed at finer particle size distributions when sound is applied.

We further examined the dependence of filtering performance on a variety of airflow scenarios. A modulated circuit and an extraction fan were connected to control the flow rate at three distinct levels: low, medium and high extraction levels. In our previous work [26], we examined the PM removal efficiencies under various flow speeds, where the air speeds were measured at the position of opening gap of acoustic trapping zone. Due to the turbulence fluctuation in the ventilation duct,

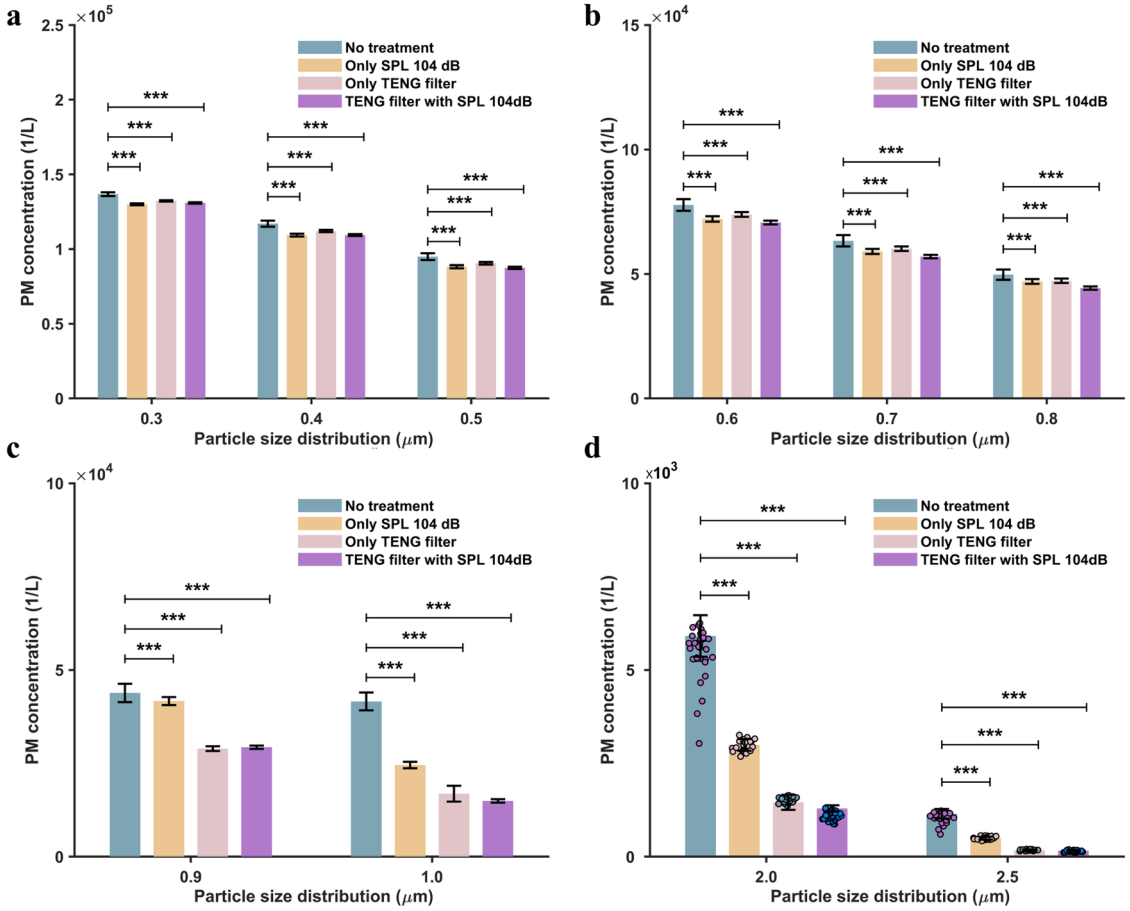

Fig. 7. A significant test of the particle concentration between the sampling data with and without air filtering treatment, where "no treatment" represents the control group without any acoustic wave or TENG filter in the U-shaped configuration. The legends of "*only SPL 104 dB*", "*only TENG filter*", and "*TENG with SPL 104 dB*" represent the outcomes of different test groups, i.e., "with acoustic treatment in SPL of 104 dB in the U-shaped configuration", "TENG placed in the U-shaped configuration without sound stimulation", and "with TENG in the U-shaped configuration and acoustic power in SPL of 104 dB", respectively. It should be noted that the symbols "*** " represents the p-value of significant level smaller than 0.01, indicating a strong significance. (a) particle size distribution of 0.3–0.5 μm, (b) 0.6–0.8 μm, (c) 0.9–1.0 μm, and (d) 2.0–2.5μm.

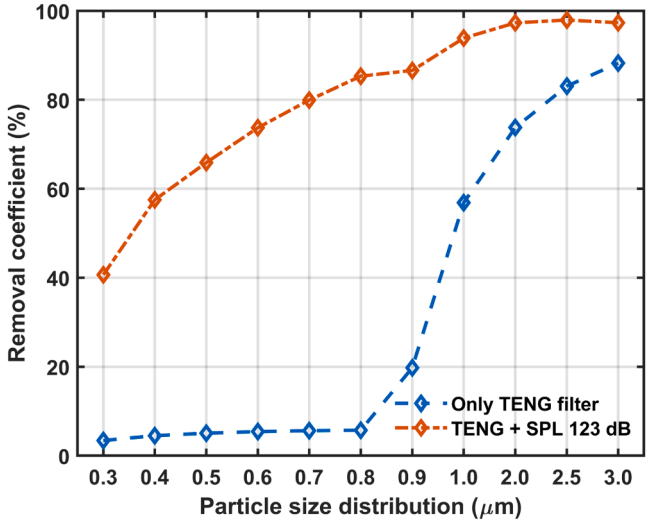

Fig. 8. Removal coefficients of PM under the scenarios of: (i) placing the TENG-S3 in the U-shaped configuration without sound stimulation; and (ii) placing the TENG-S3 in the U-shaped configuration with an SPL of 123 dB.

we measured the relevant parameters in this study by inserting a sensing probe in the ventilation duct, and the parameters of airflow including flow rate, flow speed, and temperature are presented. The measurement point was indicated in Fig. 2. In addition, the air pressure drop between the inlet and outlet of the proposed filtering system was measured to determine the quality factor (*QF*) in Eq. (4).

Fig. 11 illustrates the removal coefficients of the proposed filtering system when exposed to various flow rates at the particle size distribution of 0.3–3.0 μm. The results in Fig. 11(a)–(c) show comparable patterns. Clear evidence is that the acoustic effects considerably enhance the removal of fine particles, which is more effective under the scenario at low flowrate. The sound intensity is positively correlated with the improvement induced by acoustic effects. When the flow rate increased, the acoustic-induced gain on removal coefficients was restricted, referring to the compactness of the plotting lines in Fig. 11(a)–(c). The acoustic-induced improvement may exhibit a limited effect at this scenario since the high airflow contains a stronger carrying capacity on the suspended particles. In Fig. 11(d), the recorded details under three operating scenarios (i.e., low, medium, and high flow rates) are illustrated. The mean value of flow rates measured under three operating scenarios were 8.6 m^3/h, 4.5 m^3/h, and 1.1 m^3/h in high, medium, and low fan extraction level, respectively. The pressure drop in the ventilation duct between two sides of the filtering system was measured and calculated, as shown in Fig. 11(d). The pressure drop due to the presence of U-shaped design was ranged from 5 to 37 Pa. Comparing to existing

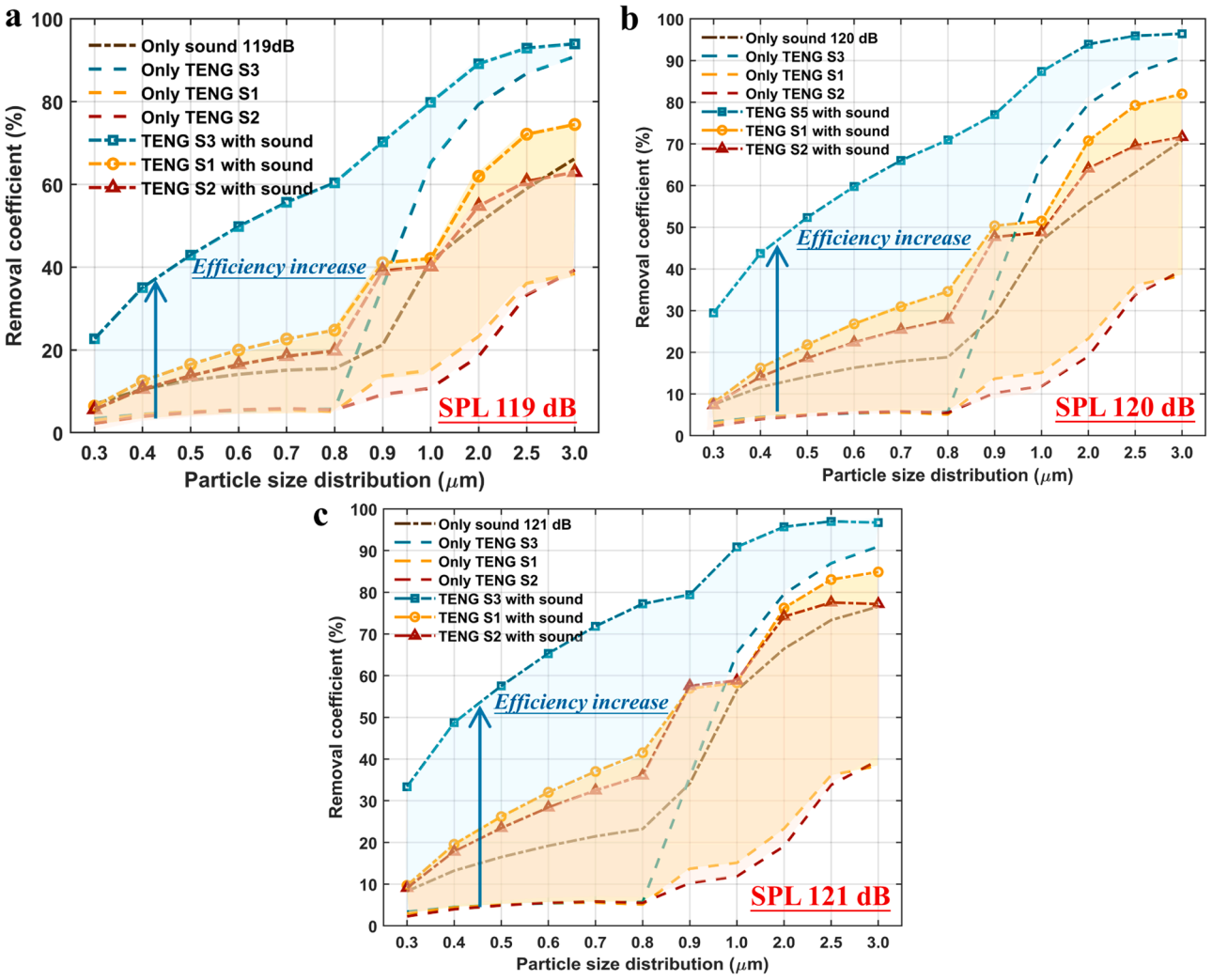

Fig. 9. Comparison of particle removal coefficients with various TENG filters (TENG-S3, TENG-S1, TENG-S2) at the particle size distribution of 0.3–3.0 μm, (a) in SPL of 119 dB, (b) in SPL of 120 dB, and (c) in SPL of 121 dB.

studies, the pressure drop was reported as 61 Pa for a polyetherimide–silica fibrous membrane filter [43], approximately 42 Pa for an electrospun CD/PLLA nanofiber filter [55], and between 5–55 Pa for an R-TENG enhanced multilayered antibacterial polyimide nanofiber filter under a gas flow of 10–60 L/min [64]. Additionally, a needle-punched TENG air filter with PTFE/PPS fibers exhibited a pressure drop of 15–60 Pa, depending on the material surface density [65]. Due to variations in measurement conditions, a comparison of quality indices regarding the performance of the filtering system is presented in the following section.

The design of the U-shaped configuration aims at forming an acoustic standing wave field, thereby facilitating acoustic-particle interaction and mutual friction of triboelectric layers. It is to improve the filtration efficiency at fine particles by maximizing the utilization of sound energy, and meanwhile it inevitably sacrifices a part of flow rate in the ventilation duct. From the aspect of qualitative analysis, the presence of the U-shaped configuration forms a complex flow field in the ventilation duct. For instance, increased airflow may enhance the interaction between the triboelectric layers and create a recirculating airflow within the resonant chambers due to turbulence effects [26]. This recirculating flow can cause some fine particles to remain within the sound pressure field for an extended interaction period, leading to a higher number of particles experiencing the trapping effect rather than being directly carried away by the airflow. On the other hand, higher airflow does indeed boost the particle-carrying capacity of the airflow, suggesting a greater likelihood of particles being expelled from the acoustic active zone compared to lower airflow rates. Consequently, the performance of the proposed system would be limited to high airflow conditions. It necessitates a quantitative analysis rather than qualitative ones. The subsequent section will further discuss the enhancement effects of U-shaped design and the trade-offs between airflow rate and sound-induced effects.

3.4. Enhancement effects of the U-shaped configuration

A comparative experiment was conducted in a straight ventilation tube (ST) with various passive membrane-types filters for comparison. TENGs were also examined in the ST as a stand-alone wind-driven type filter for PM removal. With the dynamics of airflow, the triboelectric layers can be activated under the wind-driven vibration. Besides, the layered nanofiber's morphologic structure enables the TENGs to intercept the fine particles, and the activated TENGs under wind flow can capture the surface-charged particles via electrostatic effects. For comprehensive comparison, a commercial high-efficiency particulate air (HEPA) filter (grade H12, width×length = 14 cm×14 cm) was also examined in the experiment.

Fig. 12(a)–(c) illustrate the particle matter concentrations under high, medium, and low flow rates at the particle size distribution of 0.3–3.0 μm. Fig. 12(d)–(f) shows the removal coefficients of the filtering system when placed TENG-S3 at three positions: (i) TENG-S3 as a

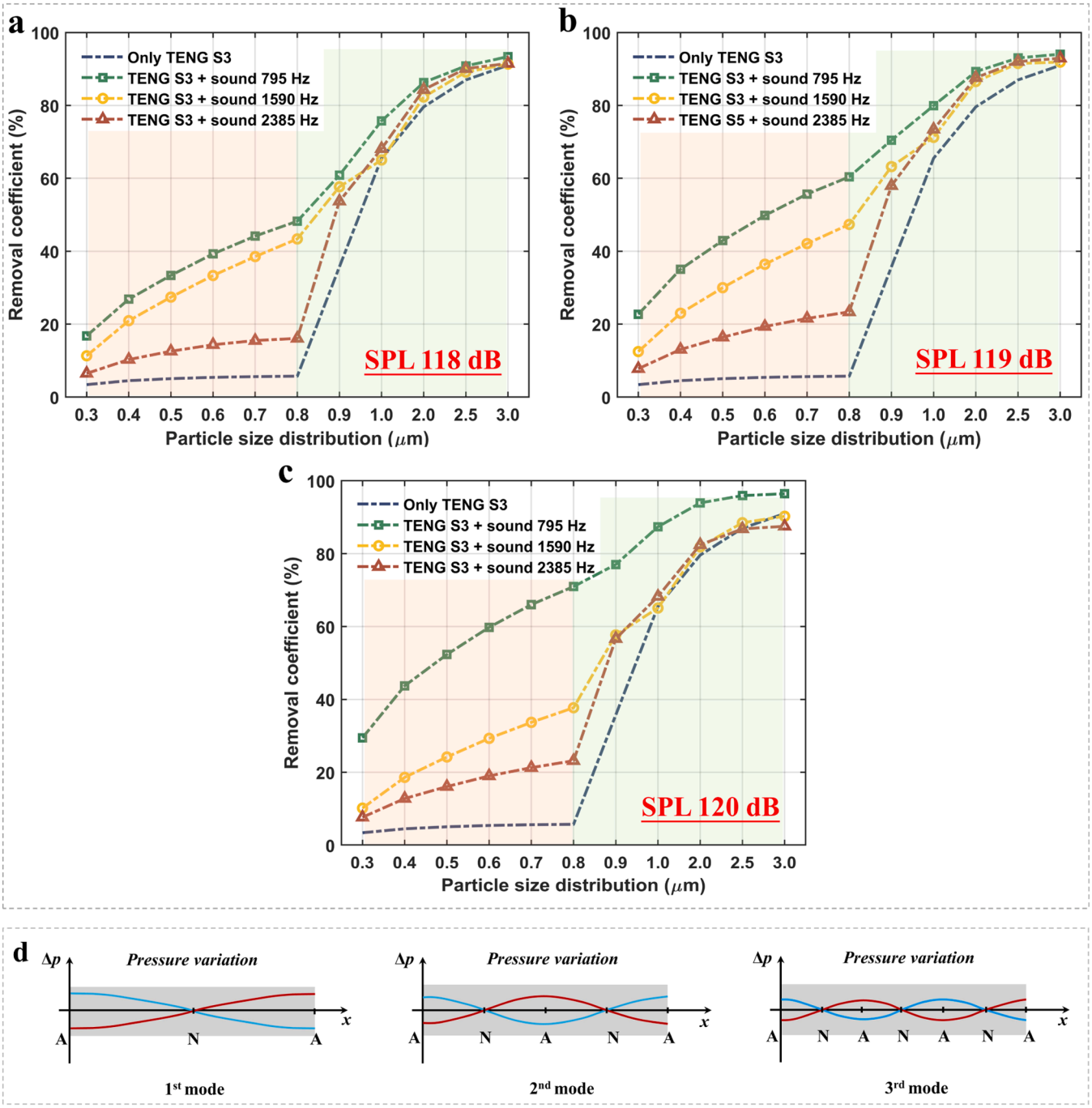

Fig. 10. Comparison of removal coefficients of particles with TENG-S3 filter at various acoustic excitation frequencies ($f_1 = 795$ Hz, $f_2 = 1590$ Hz, and $f_3 = 2385$ Hz) at the particle size distribution of 0.3–3.0 μm under (a) 118 dB; (b) 119 dB; and (c) 120 dB. (d) A simple illustration of the pressure variation in standing wave fields at the first three acoustic frequencies is presented. It is noteworthy that "A" signifies the pressure anti-node, while "N" denotes the pressure node within standing wave fields.

membrane filter attached in the straight ventilation duct; (ii) TENG-S3 as a unit attached into the U-shaped configuration without sound stimulation; and (iii) TENG-S3 as a unit placed in the U-shaped configuration with various sound excitation levels (i.e., 116 dB, 118 dB, 120 dB).

The removal coefficients can reach approximately 20 % when using the TENG unit as a membrane filter (see the blue dashed lines) in the ST measurement. In Fig. 12(d), drawing an auxiliary line at a particle size of 0.9 μm (grey dash-dot-dot line), we can use different color blocks to quantify the different treatment effects on the filtration efficiency. Comparing to yellow dash line with circular makers and orange dash-dot line, the removal coefficients of the system attaching TENGs in the U-shaped configuration with a sound stimulation (116 dB) reveal significant improvement in fine particle distribution (<0.9 μm) and limited improvement at the coarse particle distribution (>0.9 μm). In this regard, the acoustic treatment may have a greater manipulation potential for fine particles (as indicated by the light-orange color block) in Fig. 12 (d). The main difference between the two scenarios both containing similar TENGs, in contrast to the orange dash-dot line and blue dash lines, lies in the presence or absence of U-shaped configuration in the ventilation tube. A light-blue color block is utilized to denote the increase in removal coefficients with the presence of U-shaped

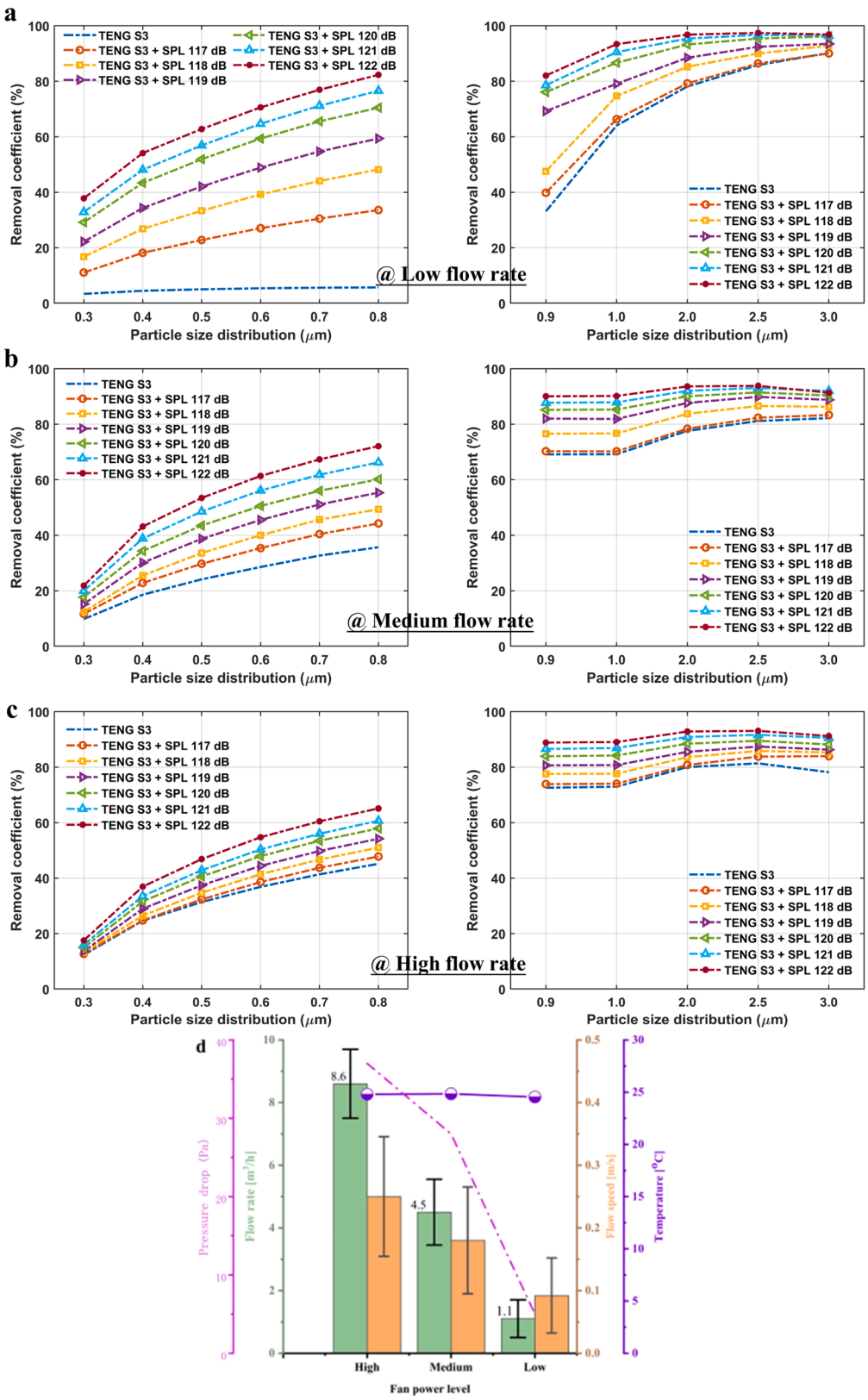

Fig. 11. Comparison of removal coefficients of proposed filtering system under various flow rates. The modulated circuit and extraction fan were responsible for regulating the flow rate. Three levels (low, medium, and high) are used to identify the power levels of the extraction fans: (a)–(c) comparison of removal coefficients under low, medium, and high flow rates, respectively, and (d) the measured flow rate, flow speed, temperature and pressure drop of the ventilation tube with the U-shaped design under three levels. The average flow rates recorded under three operating scenarios were 8.6 m^3 /h, 4.5 m^3 /h, and 1.1 m^3 /h for high, medium, and low fan extraction levels, respectively.

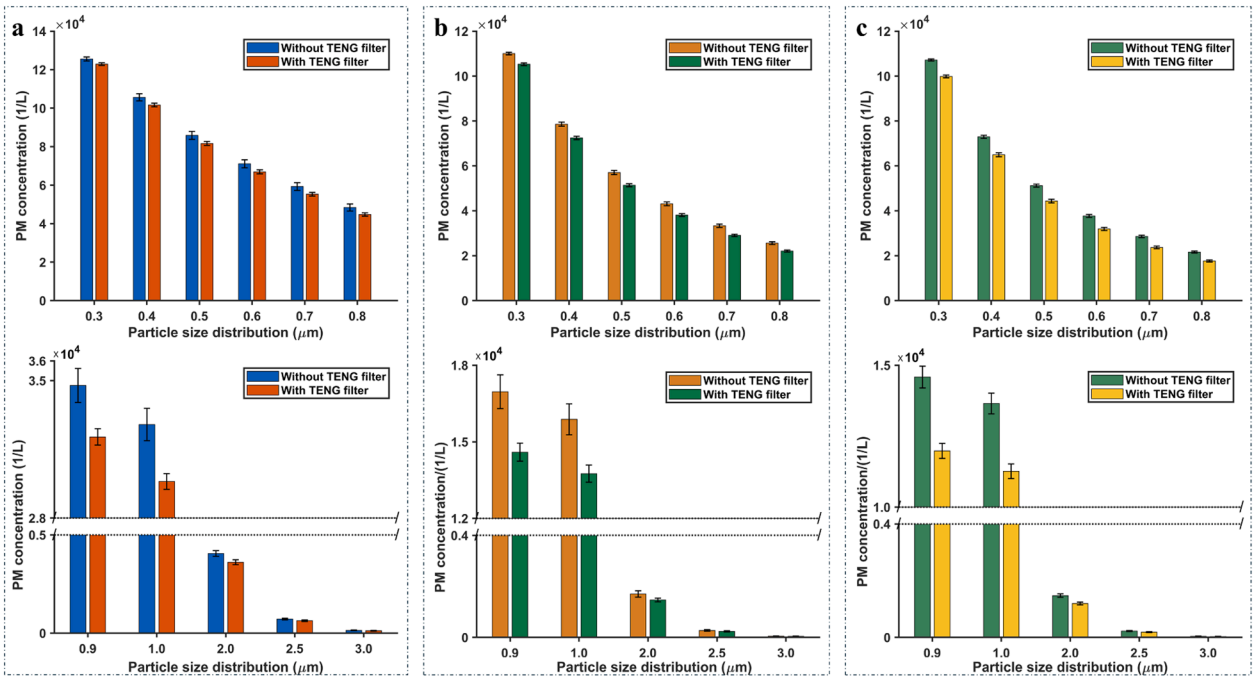

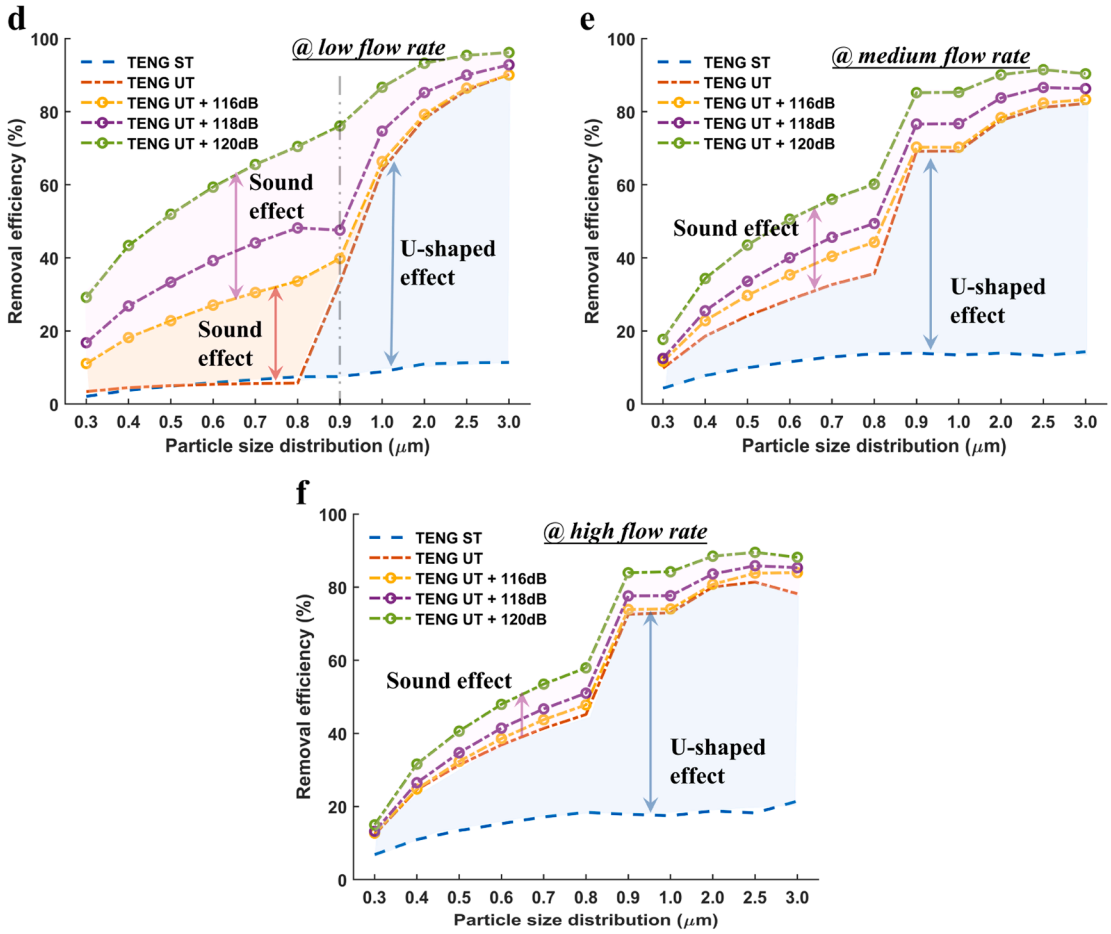

Fig. 12. Investigation of U-shaped design and sound effects on the removal coefficients under three different flow rate scenarios. (a)–(c) the variation in PM concentration of the TENG unit functioning as a standalone membrane filter in the straight tube at three different flow rates, with a particle size distribution ranging from 0.3 to 3.0 μm; (d)–(f) comparison of removal coefficients under three different flow rate scenarios: (i) TENG unit placed at the straight tube as a standalone membrane filter (TENG ST), (ii) TENG units placed in the U-shaped tube but without sound excitation (TENG UT), and (iii) TENG units placed in the U-shaped tube with sound excitation (116 dB, 118 dB, 120 dB), respectively.

configuration, whereas great effects are observed at the coarse particle distribution (>0.8 μm) and limited effects on the distribution of fine particles (<0.8 μm). As the SPL was increased from 116 dB to 120 dB, a significant enhancement in removal coefficients caused by sound waves can be observed in Fig. 12(d). This is separately indicated by the light-orange and purple color blocks, showing a stronger impact on the removal of fine particles with sound treatment.

In Fig. 12(e) and (f), the presence of a U-shaped configuration shows an apparent improvement in removal coefficients, referring to a larger coverage of light-blue color blocks. The U-shaped design promotes an increase in the removal rate through turbulence effects. The increased air flowrate enables to form an intense turbulent phenomenon within the U-shaped configuration [26], thereby facilitating a stronger particle interaction under this scenario. In the meantime, the sound effects are restricted by the increasing flow rate, as evidenced by the limited improvement in removal coefficients (refer to a decrease in coverage of light-purple color blocks in Fig. 12(e) and (f)).

3.5. Filtration performance comparison of various filters

To benchmark our results with those reported in the literature, the filtration efficiency and quality factor of the present work in comparison to other related filters are presented in Figs. 13 and 14. The proposed sound-driven TENG filtering system allows for achieving a high performance with a removal coefficient of up to 97.5 % in Fig. 13. Compared to the acoustic trapping method used as a pre-filtering technique [26], the removal coefficient obtained in this study can be improved from 61 % to 93 % for $PM_{1.0}$. In contrast to an acoustic pre-filtering system used alongside a MERV commercial filter, our current work demonstrates superior filtration performance for particle sizes of 0.3 and 0.4 μm. Additionally, with the attachment of TENGs in the resonant chambers, the removal coefficient can be further improved for the coarse particles. In comparison to the high-grade MERV-13 filter that was tested by Dols et al. [66], the efficiency of present work was also consistent with the MERV-13 filter and showed superior performance in the fine particle size distribution. Besides, the present design outperformed other membrane filters fabricated by electrospun nanofibers (e.g., P6-NFM, PLLA, CD/PLLA nanofiber membrane filters [42,55]),

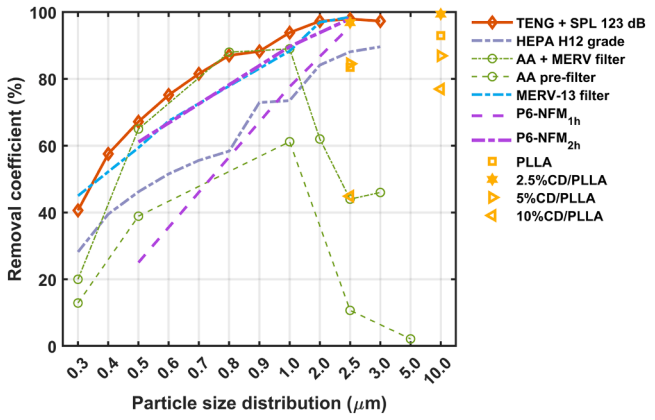

Fig. 13. Comparison of filtration performance between (i) TENG units attached in the U-shaped design with SPL in 123 dB (present work); (ii) a commercial HEPA filter (H12 grade) attached in the straight ventilation tube; (iii) acoustic trapping pre-filtering system coupled with a commercial MERV-6 filter (AA+MERV filter) [26]; (iv) acoustic trapping pre-filtering system (AA pre-filter) [26]; (v) a commercial MERV-13 filter [66]; (vi) a polyvinylidene fluoride (PVDF)/UiO-66 composite nanofiber membrane (P6-NFM) TENG filter with electrospinning time of 1 hour [42]; (vii) a P6-NFM TENG filter with electrospinning time of 2 hours [42]; (viii) a Poly(L-lactic acid) nanofibers (PLLA) membrane filter [55]; (ix) a 2.5 % Cyclodextrin/Poly(L-lactic acid) (CD/PLLA) nanofibers membrane filter [55]; (x) a 5 % CD/PLLA nanofibers membrane filter [55], (xi) a 10 % CD/PLLA nanofibers membrane filter [55].

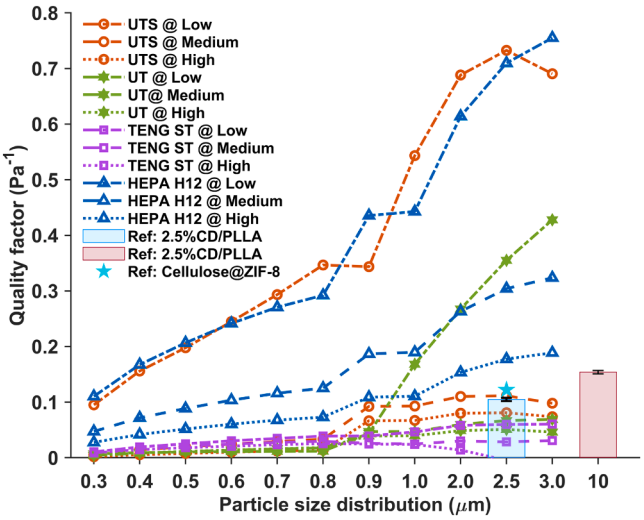

Fig. 14. Performance comparion of the quality factor between the present and available works, including: (i) TENGs attached in the U-shaped configuration with SPL in 123 dB (UTS) under low, medium, and high flow rates (orange lines with circle markers); (ii) TENGs attached in the U-shaped design without sound excitation (UT) under low, medium, and high flow rates (green lines with hexagram markers); (iii) TENGs as a membrane filter attached in the straight ventilation tube (TENG ST) under low, medium, and high flow rates (purple dash lines with square markers); (iv) a commercial product, HEPA fillter (grade H12), attached into the straight ventilation tube (HEPA H12) under low, medium, and high flow rates (blue dash lines with triangle markers); (v) bar charts of the peak quality factors of the membrane TENG filter with 2.5 % CD/PLLA electrospun nanofibers [55]; and (vi) th peak quality factors of the membrane TENG filter with cellulose air filter coated with zeolitic imidazolate frameworks (ZIFs) [67].

especially in the PM size distribution of 0.5–2.5 μm.

The quality factor (as defined in Eq. (4)) is commonly used as a metric to indicate the overall effectiveness of filters [55,67], taking into account the pressure drop induced by filters within the ventilation duct. Fig. 14 compares the quality factor of the present work with that of relevant existing publications. The results show that the proposed sound-driven TENG filtering system has a higher quality factor than other methods. The commercial HEPA (grade H12) filter also performed well, achieving a higher quality factor. Compared to the electrospun nanofibers filter [55,67], the present work demonstrates superior performance. These findings underscore the advantages of the sound-driven TENG approach developed in this study. It not only provides efficient filtration but also achieves a remarkably high-quality factor.

4. Conclusion

The implementation of a novel air filtering system can achieve high-efficiency particulate air filtration. The major findings of this work are summarized as follows:

- An acoustic-driven TENG-based particulate capturing technique has been proposed to enhance filtration efficiency for sub-micron particles (0.3–1.0 μm), marking a significant advancement over conventional air filters with its smart, controllable, and high-efficiency properties.
- To verify the effectiveness of the proposed technique, a prototype system was fabricated, and experimental tests were conducted to investigate the trapping of fine particles across various PM size ranges. Detailed parametric studies were performed concerning acoustic frequency, sound pressure level, and air flow speed. The necessity of the U-shaped configuration incorporated along a ventilation duct was also discussed.

- By facilitating acoustic agglomeration and electrostatic effects, the results demonstrate the system's ability to significantly reduce the presence of particles in the crucial sub-micron range of 0.3–3.0 μm, achieving up to a 97.5 % removal coefficient and a quality factor of 0.73 for a particle size of 2.5 μm. The present system is comparable with a HEPA filter.
- The present filtering system employs electrospun nanofibers to prepare TENGs, generating electrostatic precipitation under the acoustic effect. This approach explores the application of new nanomaterials in air purification and concurrently addresses the critical issue of requiring high sound intensity for acoustic agglomeration while maintaining low PM filtration performance.
- This innovative approach not only combines the advantages of acoustic agglomeration and electrostatic precipitation but also establishes a strategy that effectively utilizes acoustic energy and achieves high efficiency in air cleaning.

The current sound frequencies are within the audible range, yet they create a 'pure-tone' sound effect, indicating that they consist of a single frequency instead of a broadband sound effect. From a noise control viewpoint, addressing this pure-tone effect is simple with either passive or active methods in ventilation ducts. Hence, this does not pose a technical concern. Future work will focus on the inherent trade-offs between achieving high air flow rates and maintaining high particulate filtration efficiency. Additionally, the exploration of TENG-based filters with other functional capabilities (e.g., self-cleaning and virus inactivation) will be further investigated to enhance the system's performance.

CRediT authorship contribution statement

Yiting Zhang: Writing – original draft, Methodology, Investigation, Formal analysis, Data curation, Conceptualization. **Siu-Kai Lai**: Writing – review & editing, Supervision, Project administration, Methodology, Investigation, Conceptualization. **Chen Wang**: Writing – review & editing, Validation, Methodology, Investigation. **Kin-Fai Ho**: Writing – review & editing, Methodology, Investigation. **Chun H. Wang**: Writing – review & editing, Methodology, Investigation.

Declaration of Competing Interest

The authors declare that they have no known competing financial interests or personal relationships that could have appeared to influence the work reported in this paper.

Acknowledgements

The work described in this paper was supported by the General Research Fund from the Research Grants Council of the Hong Kong Special Administrative Region (Project No. PolyU 15210624), the National Natural Science Foundation of China (Grant No. 12372024), the open foundation of Provincial Collaborative Innovation Center of Mechanics of Intelligent Materials in Hebei (Grant No. KF2024003), the Natural Science Foundation of Hebei Province (Grant No. A2024203009), and the Australian Research Council through the Industrial Transformation Research Hub (Project No. IH210100040).

Data availability

Data will be made available on request.

References

[1] I. Manisalidis, E. Stavropoulou, A. Stavropoulos, E. Bezirtzoglou, Environmental and health impacts of air pollution: a review, Front Public Health 8 (2020) 14.
[2] N.T. Tung, P.C. Cheng, K.H. Chi, et al., Particulate matter and SARS-CoV-2: A possible model of COVID-19 transmission, Sci. Total Environ. 750 (2021) 141532.
[3] Y. Liu, Z. Ning, Y. Chen, et al., Aerodynamic analysis of SARS-CoV-2 in two Wuhan hospitals, Nature 582 (7813) (2020) 557–560.
[4] J. Guo, G. Chai, X. Song, X. Hui, Z. Li, X. Feng, K. Yang, Long-term exposure to particulate matter on cardiovascular and respiratory diseases in low- and middle-income countries: a systematic review and meta-analysis, Front. Public Health 11 (2023) 1134341.
[5] H. Sha, D. Qi, A review of high-rise ventilation for energy efficiency and safety, Sustain. Cities Soc. 54 (2020).
[6] T. Ahmed, P. Kumar, L. Mottet, Natural ventilation in warm climates: the challenges of thermal comfort, heatwave resilience and indoor air quality, Renew. Sustain. Energy Rev. 138 (2021) 110669.
[7] L. Morawska, J.W. Tang, W. Bahnfleth, et al., How can airborne transmission of COVID-19 indoors be minimised? Environ. Int. 142 (2020) 105832.
[8] Y. Zhang, J. Mo, Y. Li, et al., Can commonly-used fan-driven air cleaning technologies improve indoor air quality? A literature review, Atmos. Environ. 45 (26) (2011) 4329–4343.
[9] K.J. Boelter, J.H. Davidson, Ozone generation by indoor, electrostatic air cleaners, Aerosol Sci. Technol. 27 (6) (1997) 689–708.
[10] A.S. Viner, P.A. Lawless, D.S. Ensor, L.E. Sparks, Ozone generation in DC-energized electrostatic precipitators, IEEE Trans. Ind. Appl. 28 (3) (1992) 504–512.
[11] F. Memarzadeh, R.N. Olmsted, J.M. Bartley, Applications of ultraviolet germicidal irradiation disinfection in health care facilities: effective adjunct, but not stand-alone technology, Am. J. Infect. Control 38 (5 1) (2010) S13–S24.
[12] TSI Incorporated Inc., Mechanisms of filtration for high efficiency fibrous filters - Application Note ITI-041, 2012.
[13] P. Azimi, D. Zhao, B. Stephens, Estimates of HVAC filtration efficiency for fine and ultrafine particles of outdoor origin, Atmos. Environ. 98 (2014) 337–346.
[14] A. Ashrae, Standard 62.1, in: Ventilation for Acceptable Indoor Air Quality, 2019, American Society of Heating, Refrigerating, and Air-Conditioning Engineers: Atlanta, GA, USA, 2019.
[15] N. Nassif, The impact of air filter pressure drop on the performance of typical air-conditioning systems, Build. Simul. 5 (4) (2012) 345–350.
[16] T. Fazli, R.Y. Yeap, B. Stephens, Modeling the energy and cost impacts of excess static pressure in central forced-air heating and air-conditioning systems in single-family residences in the U.S, Energy Build. 107 (2015) 243–253.
[17] G. Guyot, M.H. Sherman, I.S. Walker, Smart ventilation energy and indoor air quality performance in residential buildings: a review, Energy Build. 165 (C) (2018) 416–430.
[18] A. Haake, J. Dual, Micro-manipulation of small particles by node position control of an ultrasonic standing wave, Ultrasonics 40 (1) (2002) 317–322.
[19] B.F. Ng, J.W. Xiong, M.P. Wan, Application of acoustic agglomeration to enhance air filtration efficiency in air-conditioning and mechanical ventilation (ACMV) systems, PLOS One 12 (6) (2017) e0178851.
[20] W.T. Yuen, S.C. Fu, C.Y.H. Chao, The effect of aerosol size distribution and concentration on the removal efficiency of an acoustic aerosol removal system, J. Aerosol Sci. 104 (2017) 79–89.
[21] Y. Shi, J. Wei, W. Bai, Z. Zhao, O.O. Ayantobo, G. Wang, Theoretical analysis of acoustic and turbulent agglomeration of droplet aerosols, Adv. Powder Technol. 34 (10) (2023) 104145.
[22] X. Zhang, P. Liu, G. Liu, S.H. Lim, M.P. Wan, G. Lisak, B.F. Ng, An efficient strategy to enhance air filtration through the synergistic effects of ultrasonics and seed particles, Sep. Purif. Technol. 353 (2025) 128600.
[23] Q. Zhang, Z. Wang, P. Hall, Particle agglomeration via resonant acoustic mixer for dry powder inhalation, Chem. Eng. Res. Des. 203 (2024) 253–262.
[24] J. Feng, M. Lu, K. Wang, et al., Study on the fast elimination of smoke particle based on electro-acoustic coupling agglomeration technology, Particuology 88 (2024) 1–10.
[25] Z. Mao, G. Zhang, H. Gu, D. Yuan, M. Liu, Experimental study of acoustic agglomeration coupled with water droplets on eliminating cable fire smoke, Powder Technol. 412 (2022) 117977.
[26] Y.T. Zhang, S.K. Lai, J.C.W. Yu, H. Guo, C.W. Lim, A novel U-shaped acoustic-manipulated design to enhance the performance of low-efficiency filters for sub-micron particles, Powder Technol. 392 (2021) 412–423.
[27] Y. Du, Q. Tang, W. He, et al., Harvesting ambient mechanical energy by multiple mode triboelectric nanogenerator with charge excitation for self-powered freight train monitoring, Nano Energy 90 (2021) 106543.
[28] S. Fu, H. Wu, C. Shan, et al., Ultra-durable and high-output triboelectric nanogenerator based on coupling of soft-soft contact and volume effect, Nano Energy 116 (2023) 108850.
[29] H. Yang, M. Wang, M. Deng, et al., A full-packaged rolling triboelectric-electromagnetic hybrid nanogenerator for energy harvesting and building up self-powered wireless systems, Nano Energy 56 (2019) 300–306.
[30] J. Chen, G. Zhu, W. Yang, et al., Harmonic-resonator-based triboelectric nanogenerator as a sustainable power source and a self-powered active vibration sensor, Adv. Mater. 25 (42) (2013) 6094–6099.
[31] G. Zhu, B. Peng, J. Chen, Q.S. Jing, Z.L. Wang, Triboelectric nanogenerators as a new energy technology: From fundamentals, devices, to applications, Nano Energy 14 (2015) 126–138.
[32] Q. Tang, X. Pu, Q. Zeng, et al., A strategy to promote efficiency and durability for sliding energy harvesting by designing alternating magnetic stripe arrays in triboelectric nanogenerator, Nano Energy 66 (2019) 104087.
[33] Y. Xi, J. Wang, Y. Zi, et al., High efficient harvesting of underwater ultrasonic wave energy by triboelectric nanogenerator, Nano Energy 38 (2017) 101–108.
[34] X. Ge, N. Hu, F. Yan, Y. Wang, Development and applications of electrospun nanofiber-based triboelectric nanogenerators, Nano Energy 112 (2023) 108444.

[35] C. Shan, W. He, H. Wu, et al., Efficiently utilizing shallow and deep trapped charges on polyester fiber cloth surface by double working mode design for high output and durability TENG, Nano Energy 104 (2022) 107968.
[36] X. Yan, M. Yu, S. Ramakrishna, S.J. Russell, Y.-Z. Long, Advances in portable electrospinning devices for in situ delivery of personalized wound care, Nanoscale 11 (41) (2019) 19166–19178.
[37] A. Cimini, E. Imperi, A. Picano, M. Rossi, Electrospun nanofibers for medical face mask with protection capabilities against viruses: state of the art and perspective for industrial scale-up, Appl. Mater. Today 32 (2023) 101833.
[38] X. He, J. Li, C. Wang, et al., Highly air-permeable and dust-holding protective membranes by hierarchical structuring of electroactive poly(lactic acid) micro- and nanofibers, J. Hazard Mater. 480 (2024) 136462.
[39] J. Li, X. He, L. Ke, et al., Hierarchically nano-decorated poly(lactic acid) nanofibers for humidity-resistant respiratory healthcare and high-accuracy disease diagnosis, ACS Appl. Mater. Interfaces 16 (39) (2024) 52476–52486.
[40] G. Liu, J. Nie, C. Han, et al., Self-powered electrostatic adsorption face mask based on a triboelectric nanogenerator, ACS Appl. Mater. Interfaces 10 (8) (2018) 7126–7133.
[41] Z. Shao, J. Jiang, X. Wang, W. Li, L. Fang, G. Zheng, Self-powered electrospun composite nanofiber membrane for highly efficient air filtration, Nanomaterials 10 (2020).
[42] Y. Hu, Y. Wang, S. Tian, A. Yu, L. Wan, J. Zhai, Performance-enhanced and washable triboelectric air filter based on polyvinylidene fluoride/UiO-66 composite nanofiber membrane, Macromol. Mater. Eng. 306 (8) (2021) 2100128.
[43] X. Li, N. Wang, G. Fan, J. Yu, J. Gao, G. Sun, B. Ding, Electreted polyetherimide–silica fibrous membranes for enhanced filtration of fine particles, J. Colloid Interface Sci. 439 (2015) 12–20.
[44] P.C. Sherrell, A. Šutka, M. Timusk, A. Šutka, Alternatives to fluoropolymers for motion-based energy harvesting: perspectives on piezoelectricity, triboelectricity, ferroelectrets, and flexoelectricity, Small 20 (32) (2024) 2311570.
[45] A. Al-Abduljabbar, I. Farooq, Electrospun polymer nanofibers: processing, properties, and applications, Polymers 15 (1) (2022) 65.
[46] Z. Shao, H. Chen, Q. Wang, et al., High-performance multifunctional electrospun fibrous air filter for personal protection: a review, Sep. Purif. Technol. 302 (2022) 122175.
[47] T. Lei, L. Yu, G. Zheng, L. Wang, D. Wu, D. Sun, Electrospinning-induced preferred dipole orientation in PVDF fibers, J. Mater. Sci. 50 (12) (2015) 4342–4347.
[48] Z. He, F. Rault, M. Lewandowski, E. Mohsenzadeh, F. Salaün, Electrospun PVDF nanofibers for piezoelectric applications: a review of the influence of electrospinning parameters on the β phase and crystallinity enhancement, Polymers 13 (2021).
[49] Y. He, Z. Gu, W. Lu, L. Zhang, D. Zhang, T. Okuda, C.W. Yu, Charging states on atmospheric aerosol particles affected by meteorological conditions, Particuology 52 (2020) 1–9.
[50] Y. Fang, C.K. Ao, Y. Jiang, Y. Sun, L. Chen, S. Soh, Static charge is an ionic molecular fragment, Nat. Commun. 15 (1) (2024) 1986.
[51] O. Verners, L. Lapčinskis, P.C. Sherrell, A. Šutka, Contact electrification at dielectric polymer interfaces: on bond scission, material transfer, and electron transfer, Adv. Mater. Interfaces 10 (36) (2023) 2300562.
[52] K. Shi, B. Chai, H. Zou, et al., Contact electrification at adhesive interface: boosting charge transfer for high-performance triboelectric nanogenerators, Adv. Funct. Mater. 33 (50) (2023) 2307678.
[53] D.J. Lacks, T. Shinbrot, Long-standing and unresolved issues in triboelectric charging, Nat. Rev. Chem. 3 (8) (2019) 465–476.
[54] Z. Qiao, Y. Huang, N. Vincenzo, W. Dong, Aerosol manipulation through modulated multiple acoustic wavepackets with a pair of resonators, Powder Technol. 322 (2017) 24–31.
[55] Sompit Wanwong, Weradesh Sangkhun, Pimsumon Jiamboonsri, Electrospun cyclodextrin/poly(L-lactic acid) nanofibers for efficient air filter: their PM and VOC removal efficiency and triboelectric outputs, Polymers 15 (3) (2023) 722.
[56] W.T. Yuen, S.C. Fu, C.Y.H. Chao, The correlation between acoustic streaming patterns and aerosol removal efficiencies in an acoustic aerosol removal system, Aerosol Sci. Technol. 50 (1) (2016) 52–62.
[57] V.S. Reddy, Y. Tian, C. Zhang, et al., A review on electrospun nanofibers based advanced applications: from health care to energy devices, Polymers 13 (21) (2021) 3746.
[58] H. Zou, Y. Zhang, L. Guo, et al., Quantifying the triboelectric series, Nat. Commun. 10 (1) (2019) 1427.
[59] A.V. Oppenheim, R.W. Schafer, J.R. Buck, Prentice-Hall signal processing series, in: W. Ronald, Schafer, R.Buck John (Eds.), Discrete-time signal processing / Alan V. Oppenheim, Second edition, Prentice Hall, Upper Saddle River, N.J, 1999.
[60] Q. Chang, C. Zheng, Z. Yang, M. Fang, X. Gao, Z. Luo, K. Cen, Electric agglomeration modes of coal-fired fly-ash particles with water droplet humidification, Fuel 200 (2017) 134–145.
[61] Y.T. Zhang, On Investigation of Acoustic Waves and Its Applications in Noise and Air Studies, Doctoral dissertation, Department of Civil and Environmental Engineering, 2022. The Hong Kong Polytechnic University.
[62] S.K. Lai, Y.T. Zhang, J.C.W. Yu, Y. Li, A new approach for an induced coagulation of particulate matter through thermo-acoustic agglomeration. in Proceedings of 2020 International Congress on Noise Control Engineering, Inter Noise 2020 (2020).
[63] Z. Zhang, Z. Deng, P. Luo, G. Shen, S. Zhang, Review of acoustic agglomeration technology research, ACS Omega 9 (20) (2024) 21690–21705.
[64] G.Q. Gu, C.B. Han, J.J. Tian, et al., Triboelectric nanogenerator enhanced multilayered antibacterial nanofiber air filters for efficient removal of ultrafine particulate matter, Nano Res. 11 (8) (2018) 4090–4101.
[65] Y. Wang, Y. Xu, D. Wang, et al., Polytetrafluoroethylene/polyphenylene sulfide needle-punched triboelectric air filter for efficient particulate matter removal, ACS Appl. Mater. Interfaces 11 (51) (2019) 48437–48449.
[66] W. Dols, B. Polidoro, D. Poppendieck, S. Emmerich, A Tool to Model the Fate and Transport of Indoor Microbiological Aerosols (FaTIMA). Technical Note. NIST TN 2095 National Institute of Standards and Technology, 2020.
[67] P. Sukchai, S. Wanwong, J. Wootthikanokkhan, Electrospun cellulose air filter coated with zeolitic imidazolate frameworks (ZIFs) for efficient particulate matter removal: effect of coated ZIFs on filtration performance, Fibers Polym. 23 (5) (2022) 1206–1216.